DOI: 10.1093/jnci/djq217
Advance Access publication on June 16, 2010.

ARTICLE

Essential Role of TRPC6 Channels in G2/M Phase Transition and Development of Human Glioma

Xia Ding, Zhuohao He, Kechun Zhou, Ju Cheng, Hailan Yao, Dongliang Lu, Rong Cai, Yening Jin, Bin Dong, Yinghui Xu, Yizheng Wang

Manuscript received January 17, 2009; revised July 20, 2009; accepted May 17, 2010.

Correspondence to: Yizheng Wang, PhD, Chinese Academy of Sciences, Laboratory of Neural Signal Transduction, Institute of Neuroscience, Shanghai Institute for Biological Sciences, State Key Laboratory of Neuroscience, 320 Yueyang Rd, Shanghai 200031, China (e-mail: yzwang@ion.ac.cn).

Background Patients with glioblastoma multiforme, the most aggressive form of glioma, have a median survival of approximately 12 months. Calcium (Ca^{2+}) signaling plays an important role in cell proliferation, and some members of the Ca^{2+}-permeable transient receptor potential canonical (TRPC) family of channel proteins have demonstrated a role in the proliferation of many types of cancer cells. In this study, we investigated the role of TRPC6 in cell cycle progression and in the development of human glioma.

Methods TRPC6 protein and mRNA expression were assessed in glioma (n = 33) and normal (n = 17) brain tissues from patients and in human glioma cell lines U251, U87, and T98G. Activation of TRPC6 channels was tested by platelet-derived growth factor–induced Ca^{2+} imaging. The effect of inhibiting TRPC6 activity or expression using the dominant-negative mutant TRPC6 (DNC6) or RNA interference, respectively, was tested on cell growth, cell cycle progression, radiosensitization of glioma cells, and development of xenografted human gliomas in a mouse model. The green fluorescent protein (GFP) and wild-type TRPC6 (WTC6) were used as controls. Survival of mice bearing xenografted tumors in the GFP, DNC6, and WTC6 groups (n = 13, 15, and 13, respectively) was compared using Kaplan–Meier analysis. All statistical tests were two-sided.

Results Functional TRPC6 was overexpressed in human glioma cells. Inhibition of TRPC6 activity or expression attenuated the increase in intracellular Ca^{2+} by platelet-derived growth factor, suppressed cell growth and clonogenic ability, induced cell cycle arrest at the G2/M phase, and enhanced the antiproliferative effect of ionizing radiation. Cyclin-dependent kinase 1 activation and cell division cycle 25 homolog C expression regulated the cell cycle arrest. Inhibition of TRPC6 activity also reduced tumor volume in a subcutaneous mouse model of xenografted human tumors ($P = .014$ vs GFP; $P < .001$ vs WTC6) and increased mean survival in mice in an intracranial model ($P < .001$ vs GFP or WTC6).

Conclusions In this preclinical model, TRPC6 channels were essential for glioma development via regulation of G2/M phase transition. This study suggests that TRPC6 might be a new target for therapeutic intervention of human glioma.

J Natl Cancer Inst 2010;102:1052–1068

Glioma is the most common tumor of the central nervous system and can originate from the neoplastic transformation of fully differentiated glia, neural stem cells, or progenitor cells (1). Based on the origin of the cells, glioma is classified into three main types by the World Health Organization: astrocytoma, oligodendrocytoma, and mixed oligoastrocytoma; and all types are histologically graded as 1–4 based on four main features—nuclear atypia, mitosis, microvascular enrichment, and necrosis (2). Grade 1 is usually benign and curable with complete surgical resection; grade 2 is a low-grade diffuse glioma and may progress to higher grades; higher-grade gliomas like grades 3 and 4 are malignant and have increased proliferative and invasive capacity and poor patient outcomes (2–5). Glioblastoma multiforme (GBM), a grade 4 and malignant glioma, is the most aggressive of all gliomas (4,5).

Glioma accounts for 40%–90% of all brain tumors, depending on age (6). The most common types of gliomas are malignant astrocytomas, including the anaplastic astrocytoma and GBM, but GBM constitutes more than 50% of all gliomas (3,7). Low-grade (grades 1 and 2) astrocytomas are usually reported in young adulthood and anaplastic astrocytomas in the fourth or fifth decade of life, whereas GBM is usually found in patients more than 60 years of age (3). Because of its aggressive nature, high recurrence rate, and difficulty to treat by resection and adjuvant radiotherapy or chemotherapy, the median survival time for GBM patients is approximately 12 months, compared with 5 years in patients with

low-grade glioma (3). Therefore, it is important to elucidate the mechanisms of glioma development and find key molecular targets for the development of effective therapies.

Maintenance of intracellular cation homeostasis is critical for many cellular functions (8–10). Calcium (Ca^{2+}) signaling plays an important role in cell proliferation and is required at various stages of the cell cycle (11). The signaling involves receptors, channels, transducers, Ca^{2+} effectors, Ca^{2+}-sensitive enzymes, Ca^{2+} pumps, and Ca^{2+} exchangers (8). In many forms of human cancer, the Ca^{2+} signaling proteins have abnormal expression and activity, contributing to the highly proliferative capacity of cancer cells (12,13). For example, protein kinase C and calmodulin-dependent protein kinase have been suggested as therapeutic targets for cancers (14,15).

Ca^{2+} entry through Ca^{2+}-permeable channels activates intracellular Ca^{2+} effectors and Ca^{2+}-sensitive enzymes, which in turn mediate cellular activities necessary for cell cycle progression and cell proliferation (13). In tumor cells, abnormal expression of Ca^{2+} channel proteins has been shown to contribute to malignant proliferation (13). At least two types of Ca^{2+} channels, the T-/L-type voltage-gated Ca^{2+} channels (VGCC) and transient receptor potential (TRP) channels, are known to have a functional role in the development of human tumors (16–18). The T-type VGCC was shown to be important for the proliferation of esophageal cancer cells, and the L-type VGCC expression was shown elevated in colon cancer (16,18).

The TRP channels are a superfamily of nonselective cation channels that were initially identified in *Drosophila melanogaster* (19). The mammalian homologs are categorized into seven families according to sequence homology—TRPC (canonical), TRPV (vanilloid), TRPM (melastatin), TRPA (ankyrin), TRPP (polycystin), TRPN (Nompc), and TRPML (mucolipin) (19). Most of the TRP channels are permeable to Ca^{2+} and sodium, whereas TRPM6 and 7 channels are permeable to magnesium (19).

The Ca^{2+}-permeable TRPC subfamily contains seven members (TRPC1–7), and based on the amino acid similarities, the human TRPCs are divided into three subgroups—TRPC1, TRPC3/6/7, and TRPC4/5; TRPC2 being a pseudogene (19). These channels play an important role in many physiological and pathological processes (17,20,21). For example, TRPC1, 3, and 6 have demonstrated a role in tumor cell proliferation. TRPC1 and 3 are involved in proliferation of breast and ovarian cancer cells, respectively (22,23). TRPC6 is involved in proliferation of liver, prostate, breast, and brain tumor cells (24–27).

TRPC3 and 6 channels are activated either by a receptor-operated pathway or a store-operated pathway (19,28). The receptor-operated pathway is activated by G-protein–coupled receptors or receptor tyrosine kinases through a phospholipase C–dependent generation of diacylglycerol and inositol 1,4,5-triphosphate (IP_3). Diacylglycerol can directly activate TRPCs to regulate Ca^{2+} signaling (28). The store-operated pathway activates TRPCs when there is an IP_3 receptor–dependent release of intracellular Ca^{2+}, which results in influx of extracellular Ca^{2+} into the cell via TRPCs (28,29). Both the receptor-operated pathway and the store-operated pathway play an important role in cell proliferation (30–33).

TRPC3- and 6-mediated Ca^{2+} signaling activates the calmodulin-dependent protein kinase (34,35) and mitogen-activated protein kinase (36), which are important for cell proliferation and cell cycle (11,37). Calmodulin-dependent protein kinase II activates cell division cycle 25 homolog C (CDC25C) (38), an essential phosphatase for Gap 2 (G2) to mitotic (M) phase transition in the cell cycle. CDC25C in turn dephosphorylates and activates a member of the cyclin-dependent protein kinases and a central regulator of G2/M phase transition—cyclin-dependent kinase 1 (CDK1), also known as cell division cycle 2 (39).

In this study, we examined whether TRPC3 and 6 channels play an important role in glioma development via regulation of cell cycle progression. We studied the expression of channel proteins in human glioma samples and analyzed the phenotypes after inhibiting TRPC channels in human glioma cell lines both in vitro and in vivo.

CONTEXT AND CAVEATS

Prior knowledge

The median patient survival in glioblastoma multiforme, the most aggressive of all gliomas, is approximately 12 months. It is not known whether abnormal calcium signaling, which is often implicated in the development of cancers, plays an important role in the development of gliomas.

Study design

The role of calcium-permeable transient receptor potential canonical 6 (TRPC6) channel was examined in glioma cell growth, cell cycle progression, antigrowth effect of ionizing radiation, development of xenografted gliomas in mice, and survival of glioma-bearing mice.

Contribution

Inhibition of TRPC6 activity showed reduced cell growth, cell cycle arrest in the G2 phase, and enhanced antiproliferative effect of ionizing radiation in vitro, as well as reduced growth of subcutaneously and intracranially implanted gliomas and increased survival in mice in vivo.

Implications

TRPC6 channels are involved in glioma development and could be a therapeutic target to treat human glioma.

Limitations

Whether inhibition of TRPC6 activity increased the radiosensitivity of intracranial gliomas was not demonstrated. This study used a mouse model and the results may be different in humans.

From the Editors

Materials and Methods

Cell Culture and Reagents

Because of the heterogeneous nature of tumors, three human glioma cell lines (U-251 MG [U251], U-87 MG [U87], and T98G) and one rat glioma cell line (C6) were used. U251 and T98G have mutated tumor protein p53 and mutated phosphatase and tensin homolog; U87 and C6 have wild-type tumor protein p53 and mutated phosphatase and tensin homolog (40–44). All cell lines were purchased from American Type Culture Collection (ATCC, Manassas, VA). HeLa cells, human embryonic kidney (HEK) 293

cells, and HEK293T cells were also purchased from ATCC. Phenotypes of each cell line were compared with the typical cell morphology on the ATCC Web site to verify authenticity. Cells were cultured in Dulbecco's modified Eagle medium (DMEM) (Invitrogen, Carlsbad, CA), supplemented with 10% fetal bovine serum (Thermo Fisher Scientific, Inc, Waltham, MA) and antibiotics (penicillin and streptomycin, 50 units/mL each) (Invitrogen). Cells were grown in a humidified incubator with 5% CO_2 at 37°C. Other reagents were purchased: SKF96365, a nonselective inhibitor of Ca^{2+} channels (Merck KGaA, Darmstadt, Germany); mibefradil, a selective T-type Ca^{2+} channel blocker, and cyclopiazonic acid, a specific inhibitor of Ca^{2+}-ATPase of the endoplasmic reticulum (45) (Sigma-Aldrich Co, St Louis, MO); platelet-derived growth factor-BB, a member of the PDGF ligand family that can interact with all types of PDGF receptors (32) (Roche, Basel, Switzerland); and Ca^{2+}-free DMEM (Invitrogen). All other reagents were purchased from Shanghai Sangon Biological Engineering Technology & Services Co, Ltd (Shanghai, China) unless otherwise specified.

Glioma and Normal Human Brain Tissues

Surgically removed human glioma tissue samples and normal brain tissues were obtained frozen or paraffin-embedded from Ruijin Hospital and Renji Hospital, Shanghai Jiaotong University (Shanghai, China). Gliomas were graded by the Pathology Department from Renji Hospital based on the World Health Organization grading system—presence and absence of nuclear atypia, mitosis, microvascular enrichment, and necrosis (4). Human normal brain tissues (mostly from the cortex) were obtained from patients with physical injuries to the brain. These specimens were collected from the patients registered at the above-mentioned hospitals, and written informed consent was obtained from the patients. The use of human tissues was approved by the ethics committees of the hospitals.

Antibodies

The following antibodies were purchased—rabbit polyclonal anti-TRPC6 (1:400 dilution; Alomone labs, Jerusalem, Israel, and Sigma-Aldrich Co); anti-CACNA1G (α1G subunit of T-type VGCCs, 1:300 dilution; Alomone labs); anti-CDK1 and anti-phosphorylated CDK1 (tyrosine15 [Y15]) (1:1000 dilution; both from Cell Signaling Technology, Danvers, MA); anti-phosphorylated H3F3A (histone H3, Serine10 [S10]), a well-defined M phase marker (46) (1:1000 dilution; Millipore, Billerica, MA); mouse monoclonal antineuronal nuclei (NeuN) (1:1000 dilution; Millipore); anti-CDC25A and anti-CDC25C (1:1000 dilution; both from Abcam, Cambridge, UK); anti-CDC25B (1:1000 dilution; Santa Cruz Biotechnology, Santa Cruz, CA); anti-ACTB (β-actin), anti-TUBA1A (tubulin, α1A), and anti-GAPDH (glyceraldehyde-3-phosphate dehydrogenase) (1:2000 dilution; all from Sigma-Aldrich Co). All above-mentioned antibodies can detect targets from human, rat, and mouse.

We generated anti-TRPC3 antibody in our laboratory by immunizing rabbits with the antigenic peptide HKLSEKLNPSVLRC, which corresponds to residues 822–835 of mouse TRPC3 (Swiss-Prot accession Q9QZC1). The specificity of this antibody to human TRPC3 (1:500 dilution) was verified and shown in Supplementary Figure 1, A and B (available online).

Horseradish peroxidase–conjugated secondary antibodies, polyclonal goat anti-rabbit IgG, and goat anti-mouse IgG were used at 1:5000 dilution (antibodies from GE Healthcare, Bucks, UK). Texas-Red–conjugated goat anti-rabbit IgG (Invitrogen), Alexa Fluor 488 goat anti-rabbit IgG (Invitrogen), and Cy5-conjugated goat anti-mouse IgG (GE Healthcare) were used at 1:3000 dilution.

Immunoblot, Immunofluorescence, and Immunohistology

Total proteins were extracted from normal or malignant brain tissues using the radioimmunoprecipitation assay buffer (150 mM NaCl, 5 mM EDTA, 1% Triton X-100, 1 mM sodium orthovanadate, 50 mM NaF, 1 mM phenylmethanesulfonyl fluoride, 1 mM aprotinin, 1 mM leupeptin, 5 mM dithiothreitol, and 10 mM Tris–HCl [pH 7.4]). Total proteins were extracted from cells (U251, U87, T98G, C6, HeLa, and HEK293) cultured in vitro using sodium dodecyl sulfate lysis buffer (2% sodium dodecyl sulfate, 10% glycerol, 0.1 mM dithiothreitol, and 0.2 M Tris–HCl [pH 6.8]). Protein lysates were subjected to sodium dodecyl sulfate–polyacrylamide gel electrophoresis, then transferred to polyvinylidene difluoride membrane of 0.45-μm pore size (GE Healthcare), and probed with primary antibodies at 4°C overnight and secondary antibodies at room temperature for 1 hour. Bound antibodies were detected by the ECL immunoblotting detection reagent (GE Healthcare) and exposed to x-ray films. Band densities were quantified by ImageQuant software (GE Healthcare), and the densitometric results are shown. The relative amount of proteins was determined by normalizing the densitometry value of interest to that of the internal loading control and the external control.

To stain the mitotic cells by using indirect immunofluorescence, 5×10^4 U251 cells were seeded on 12-mm-diameter coverslips, fixed by 4% paraformaldehyde, permeabilized by 0.1% Triton X-100, and blocked in phosphate-buffered saline (PBS) (137 mM NaCl, 2.7 mM KCl, 10 mM Na_2HPO_4, 2 mM KH_2PO_4, pH 7.4) containing 5% bovine serum albumin (Sigma-Aldrich Co). The cells were incubated with anti-phosphorylated H3F3A (S10) at 4°C overnight, washed with PBS containing 0.5% Tween 20 (Shanghai Sangon Biological Engineering Technology & Services Co, Ltd), and incubated with Texas-Red–conjugated goat anti-rabbit IgG at room temperature for 1 hour. Nuclei (DNA) were counterstained by Hoechst 33258 (Sigma-Aldrich Co). Cells were observed under Olympus IX-51 inverted microscope (Olympus, Tokyo, Japan), and images were taken using a mercury arc lamp with barrier filters of 420, 495–540, or 575–625 nm for observing the fluorescence of Hoechst 33258, green fluorescent protein (GFP), or Texas-Red, respectively. The number of phosphorylated H3F3A (S10)-positive cells and total cell number in the same image were counted. Mitotic index was calculated as the percentage of phosphorylated H3F3A (S10)-positive cells in total cells. In each experiment, at least 2000 total cells were counted from at least three images in each group.

Immunofluorescence on cryosections was performed after sections were fixed with 4% paraformaldehyde. After washing in PBS, sections were blocked with horse serum (HyClone, Logan, UT) and incubated with TRPC6 and NeuN antibodies at 4°C overnight. Secondary antibodies were Alexa Fluor 488 goat anti-rabbit IgG (Invitrogen) together with Cy5-conjugated goat anti-mouse

IgG (GE Healthcare). Sections were counterstained by Hoechst 33258 and observed under a ZEISS LSM 510 inverted confocal microscope (Carl Zeiss MicroImaging, Inc, Thornwood, NY).

For immunohistological staining, 5-μm thickness paraffin-processed sections were mounted on poly-D-lysine–coated glass slides (Shanghai Long Island Biotech, Inc, Shanghai, China). Each slide was dewaxed in 100% xylene and rehydrated by incubation in decreasing concentrations (100%, 95%, and 75%) of alcohol. Sections were incubated in 3% hydrogen peroxide to quench endogenous peroxidase. Sections were digested in antigen retrieval buffer (50 mM Tris–HCl [pH 8.0] and 5 mM EDTA) with proteinase K (Merck KGaA) at a final concentration of 10 μg/mL. The immunoreactions were performed with VECTASTAIN Elite ABC Kit (Vector Laboratories, Burlingame, CA). Briefly, sections were blocked with horse serum and incubated overnight with diluted TRPC6 antibody at 4°C. The specificity of this antibody was confirmed in our previous study (35). Following washes with PBS, the slides were incubated with the appropriate biotinylated anti-rabbit IgG secondary antibodies (Vector Laboratories) at room temperature for 1 hour, washed, and incubated with horseradish peroxidase–conjugated streptavidin (Vector Laboratories). Sections were developed using a peroxidase substrate 3,3′-diaminobenzidine kit (Vector Laboratories) and counterstained with hematoxylin to stain the nucleus. Sections were dehydrated by incubating in increasing concentrations (75%, 95%, and 100%) of alcohol and in 100% xylene before coverslips were mounted onto the sections. Serial sections of the samples were also subjected to hematoxylin and eosin staining.

TRPC6 immunostaining was scored based on the relative intensity and area of the brown-colored 3,3′-diaminobenzidine signal. TRPC6 immunostaining was divided into three levels: strong (+++, at least 70% of the sections showed deep brown color), moderate (++, at least 70% of the sections showed moderate brown color), and weak (+, at least 70% of the sections showed light brown color) as suggested previously (47–49) and by pathologists in the hospitals. To compare normal and malignant tissues in the same patient, we defined "para-tumor tissues" as normal brain tissues adjacent to surgically removed tumor tissues. Para-tumor tissues had normal cell density and well-differentiated cell types without nuclear atypia, mitosis, microvascular enrichment, or necrosis.

In Situ Hybridization

The probe sequence targeting 443–1436 bases of the human TRPC6 mRNA (GenBank accession NM_004621) was amplified by polymerase chain reaction (PCR) (DNA Engine Peltier Thermal Cycler; Bio-Rad Laboratories, Hercules, CA) using human TRPC6 cDNA (OriGene Technologies, Rockville, MD) as the template. PCR conditions were as follows: 95°C, 5 minutes; 95°C, 30 seconds; 60°C, 30 seconds; 72°C, 1 minute, and an additional 32 cycles; 72°C, 10 minutes. Purified PCR product (with single 3′-A overhangs at both ends) was directly ligated into a pGEM-T vector (with single 3′-T overhangs at both ends) (Promega, Madison, WI). To generate the sense probe (negative control), the recombinant plasmid was linearized by *Nco*I (New England Biolabs, Ipswich, MA) and an in vitro transcription was performed by using SP6 RNA polymerase (Roche Applied Science, Bavaria, Germany). To generate the antisense probe, the plasmid was linearized by *Sac*I (New England Biolabs) and an in vitro transcription was performed by T7 RNA polymerase (Roche Applied Science). Both the sense and antisense probes were labeled with digoxigenin. Hybridization was performed on 8-μm cryosections of freshly frozen tissues. Sections were immersed in hybridization solution (50% formamide, 5× saline sodium citrate buffer [0.75 M NaCl and 75 mM sodium citrate, pH 7.0], 50 μg/mL yeast tRNA [Invitrogen], 100 μg/mL heparin, 1× Denhardt solution, 0.1% 3-[{3-cholamidopropyl} dimethylammonio]-1-propanesulfonate [CHAPS; Sigma-Aldrich Co], 0.1% Tween 20, and 5 mM EDTA) and hybridized at 65°C for 16 hours with sense or antisense probe at a concentration of 1–2 μg/mL. Posthybridization washes were performed three times in 2× saline sodium citrate at 37°C for 5 minutes and twice in 0.2× saline sodium citrate at 65°C for 30 minutes. The hybridized probes were detected using alkaline phosphatase–conjugated anti-digoxigenin Fab fragments (Roche Applied Science) and 5-bromo-4-chloro-3-indolyl phosphate/nitro blue tetrazolium (Roche Applied Science).

Adenoviral and Lentiviral Vectors

The GFP, dominant-negative form of human TRPC6 (DNC6), and wild-type TRPC6 (WTC6) were cloned into an adenoviral vector pAdEasy-1 with the cytomegalovirus promoter using the AdEasy Adenoviral Vector System Kit (Agilent Technologies, Stratagene, La Jolla, CA). Adenovirus was amplified in HEK293 cells and purified using Adeno-X Virus Mini Purification Kit (Clontech, Mountain View, CA). In DNC6, three mutations (L678A, F679A, and W680A) were introduced in the pore region of TRPC6 by PCR-mediated mutagenesis (QuikChange Site-Directed Mutagenesis Kit; Agilent Technologies, Stratagene) to block Ca^{2+} influx via TRPC6 (50). Both DNC6 and WTC6 had a GFP-tagged internal ribosome entry site for monitoring infection efficiency. In all the experiments, U251, U87, and T98G cells were infected at a multiplicity of infection (MOI) of 10, unless otherwise noted. At this dose, 48–72 hours after infection, most of the cells were GFP positive, and both the DNC6 and WTC6 were well expressed, shown in Supplementary Figure 2, A–C (available online).

Two specific sequences of short hairpin RNA (shRNA) targeting different regions of human TRPC6 mRNA sequence (shTRPC6-1 and -2, designed to rule out any nonspecific effect), a scrambled shRNA (based on shTRPC6-1), a specific sequence of shRNA targeting human CACNA1G (T-type VGCC), and a nonsense shRNA were constructed into the pLentiLox3.7 (pLL3.7) lentiviral vector (51), which had a GFP tag. The lentivirus was packaged and amplified in HEK293T cells. The U251 cells were infected at an MOI of 5, unless otherwise noted. The shRNA sequences targeting human TRPC6 and CACNA1G are described below.

shRNA Against Human TRPC6 and Human CACNA1G (T-Type VGCC)

The shRNA sequences (5′–3′) targeting human TRPC6 and human CACNA1G are listed below. Target sequences are underlined.

shTRPC6-1, forward:
TGAATGCCACTCACTCAACGTTCAAGAGA-CGTTGAGTGAGTGGCATTCTTTTTTC;
shTRPC6-1, reverse:

TCGAGAAAAAAGAATGCCACTCACTCAACG-
TCTCTTGAACGTTGAGTGAGTGGCATTCA;
shTRPC6-2, forward:
TGGACTTGACGAAAGTAACATTCAAGAGA-
TGTTACTTTCGTCAAGTCCTTTTTTC;
shTRPC6-2, reverse:
TCGAGAAAAAAGGACTTGACGAAAGTAACA-
TCTCTTGAATGTTACTTTCGTCAAGTCCA;
Scrambled shRNA (based on shTRPC6-1), forward:
TGACGTAACCTACATACCCGTTCAAGAGA-
CGGGTATGTAGGTTACGTCTTTTTTC;
Scrambled shRNA (based on shTRPC6-1), reverse:
TCGAGAAAAAAGACGTAACCTACATACCCG-
TCTCTTGAACGGGTATGTAGGTTACGTCA;
Nonsense shRNA, forward:
TGTTCTCCGAACGTGTCACGTTCAAGAGA-
CGTGACACGTTCGGAGAACTTTTTTC;
Nonsense shRNA, reverse:
TCGAGAAAAAAGTTCTCCGAACGTGTCACG-
TCTCTTGAACGTGACACGTTCGGAGAACA;
shCACNA1G, forward:
TGATCTGCAACTACATCTTCTTCAAGAGA-
GAAGATGTAGTTGCAGATCTTTTTTC; and
shCACNA1G, reverse:
TCGAGAAAAAAGATCTGCAACTACATCTTC-
TCTCTTGAAGAAGATGTAGTTGCAGATCA

Ca^{2+} Imaging

Changes in intracellular Ca^{2+} concentration $[Ca^{2+}]_i$ were measured using Fura-2 AM (Invitrogen). A total of 5×10^4 U87 cells were seeded on coverslips and incubated with 2 μM Fura-2 AM at 37°C for 30 minutes. Cells were washed three times with normal extracellular solution (120 mM NaCl, 6 mM KCl, 2 mM $CaCl_2$, 2 mM $MgCl_2$, 12 mM glucose, 12 mM sucrose, and 10 mM HEPES-free acid [pH 7.4]) or with zero Ca^{2+} extracellular solution (120 mM NaCl, 6 mM KCl, 2 mM $MgCl_2$, 12 mM glucose, 5 mM EGTA, and 10 mM HEPES-free acid [pH 7.4]) and imaged using a Nikon Eclipse Te2000-E microscope (Nikon Corporation, Tokyo, Japan) with dual excitation wavelengths for Fura-2 AM at 340 and 380 nm and detection of fluorescent emission at 500 nm. The ratio (R) of the emission at 500 nm induced by 340 and 380 nm excitation was captured at 6-second intervals. The ΔR/R was calculated as follows: $(R - R_{baseline})/R_{baseline}$. $R_{baseline}$ was the mean value of R during the pretreatment time frame (baseline) in each experiment, and ΔR was the R value at each time point of the entire experiment subtracted by the corresponding $R_{baseline}$ (36). The ΔR/R area was defined as the area of the $[Ca^{2+}]_i$ elevation curve within a given period.

Cell Growth Assay

Cell growth assays were used to study the effect of TRPC6 on glioma cell proliferation. The growth of U251, U87, and C6 cells was estimated by determination of cell growth curves or colony formation assays.

Cell growth curves were estimated by counting cell numbers by using a Beckman particle counter (Beckman Coulter, Brea, CA) every 12 or 24 hours after adenoviral infection or treatment with inhibitors. Cell numbers at individual time points were normalized to those at 0 hour in each group. Data were obtained from three independent assays performed in duplicate.

For colony formation assays using DNC6, we seeded cells at a density of 1×10^4 in a 60-mm dish and infected with adenovirus at an MOI of 10, as mentioned earlier. For colony formation assay using shTRPC6, we seeded cells at a density of 2×10^3 per well in a six-well plate 72 hours after lentiviral infection (>90% of the cells were GFP positive after 72 hours of infection). After 14 days of seeding, we stained the colonies with 0.5% crystal violet. Quantification of the colonies was obtained by measuring the optical density at 595 nm (OD_{595}) after digesting the colonies in each dish or well with 1 mL of 10% acetic acid. The OD_{595} values of DNC6- or WTC6-infected colonies were normalized to that of GFP-infected colonies. The OD_{595} values of shTRPC6-1- or shTRPC6-2-infected colonies were normalized to that of scrambled shRNA-infected colonies. Four independent experiments using either DNC6 or shTRPC6 were performed in duplicate.

Reverse Transcription–Polymerase Chain Reaction and Quantitative Real-Time PCR

Total RNA of U251, U87, T98G, and C6 cells was extracted using the Trizol reagent (Invitrogen). First-strand cDNA was synthesized in a 20 μL reaction volume containing 5 μg RNA, random hexamer, dNTP, and M-MuLV reverse trancriptase (Fermentas, Ontario, Canada). PCR using DNA Engine Peltier Thermal Cycler (Bio-Rad Laboratories) conditions were as follows: 95°C, 5 minutes; 95°C, 30 seconds; 60°C, 30 seconds; 72°C, 45 seconds, and an additional 25 cycles (for CDC25 isoforms) or 32 cycles (for TRPC isoforms); 72°C, 10 minutes.

Quantitative real-time PCR (qPCR) was performed with SYBR Premix Ex Taq Kit (TaKaRa Biotechnology, Dalian, China) and analyzed on ABI PRISM 7000 Sequence Detection System (Applied Biosystems, Foster City, CA). The qPCR conditions were as follows: 95°C, 5 minutes; 95°C, 30 seconds; 60°C, 30 seconds, 72°C, 31 seconds, and an additional 39 cycles. The qPCR results are presented as threshold cycle (Ct) value, and the relative mRNA level of interest was analyzed by normalizing the Ct value to that of the internal loading control and the external control.

Primers are listed in Supplementary Table 1 (available online).

Flow Cytometry to Examine Cell Cycle Progression

Flow cytometry assays were used to study the effect of TRPC6 or T-type VGCC on cell cycle progression. U251 cells were harvested and fixed with 75% alcohol overnight at −20°C, were washed in PBS, and treated with RNase A (Sigma-Aldrich Co) at 0.2 mg/mL and propidium iodide at 10 μg/mL at 37°C for 1 hour. In each sample, 2×10^4 cells were assayed on FACSCalibur (Becton-Dickinson, Franklin Lakes, NJ) and cell cycle phase distributions were analyzed by CellQuest Pro software (Becton-Dickinson).

Transient Transfection of Glioma Cells With CDC25C and Small Interfering RNAs

Transfection of T98G glioma cells with CDC25C construct and transfection of U87 glioma cells with small interfering RNAs targeting human TRPC6 were performed using the FuGENE HD

transfection reagent (Roche Diagnostics, Mannheim, Germany) according to the manufacturer's instructions. The CDC25C construct was generated by cloning the human CDC25C cDNA (Shanghai GeneChem Co, Ltd, Shanghai, China) into the pShuttle-cytomegalovirus vector (Agilent Technologies, Stratagene) at the *Kpn*I and *Hin*dIII restriction sites. The working concentration for each small interfering RNA was 1.5 μg/mL, and the transfections were performed three times independently.

Radiation Exposure

This assay was performed to test whether inhibition of TRPC6 activity radiosensitizes glioma cells. U251 cells treated with 10 μM SKF96365 for 24 hours or infected with DNC6 adenovirus at an MOI of 2 for 72 hours were irradiated using the 6 MeV electrons (Elekta Precise, Stockholm, Sweden) at doses of 2, 4, 6, and 8 Gy. Nonirradiated cells were treated identically as the irradiated cells, except for irradiation exposure. After irradiation, the cells were seeded at a density of 1×10^4 cells per well in a six-well plate in duplicate. After 9–15 days, colonies were stained and quantified as mentioned earlier in the cell growth assay section. Surviving fraction of cells was determined as the OD_{595} values normalized to that of nonirradiated colonies. For both SKF96365 and DNC6, five independent experiments were performed.

In Vivo Studies

This assay was to study the effect of TRPC6 activity on glioma development in vivo. In the subcutaneous glioma xenograft model, U87 cells were infected with adenovirus at MOI of 10 (GFP, DNC6, or WTC6), and 24 hours after infection when 90% of the cells were GFP positive, cells were suspended at a density of 1×10^6 per 100 μL DMEM (without antibiotics), and 2×10^6 cells were subcutaneously injected into the flank of BALB/c athymic nude male mice (SLAC Laboratory Animal, Shanghai, China), 3–4 weeks old (n = 7 per group). We measured the length (L) and width (W) of xenografted tumors every 5 days. Tumor volume was calculated as follows: $L \times (W)^2/2$.

In the intracranial glioma model, U87 cells were similarly infected with adenovirus at MOI of 10 (GFP, DNC6, or WTC6), and 24 hours after infection, 5×10^5 cells were suspended in 5 μL Leibovitz L-15 medium (without serum or antibiotics and with 2 mM L-glutamine) (Invitrogen). Cells were injected into the right caudate putamen of athymic nude male mice, 6 weeks old (n = 13–15 per group). Briefly, a 0.5- to 0.8-mm burr hole was made 2 mm right to the midline and 1 mm anterior to the bregma before the cells were stereotactically injected by a 50-μL syringe and 23-gauge needle (0.6 mm diameter) to a depth of 3 mm. Cells were injected at a speed of 1 μL/min. After 20 days of implantation (at this time point, the size of xenografted gliomas was appropriate for observation), mice were anesthetized with chloral hydrate and perfused by 4% paraformaldehyde, and their brains were removed for cryosections at 20 μm per slice for hematoxylin and eosin staining.

All athymic nude mice were kept in specific pathogen-free conditions (52), and their care was in accord with the animal welfare guidelines of the Institute of Neuroscience, Chinese Academy of Sciences.

Statistical Analysis

Statistical analysis for protein and mRNA levels, cell growth, flow cytometry, mitotic index, Ca^{2+} imaging, and in vivo tumor growth were performed using a two-sided Student t test. Based on previous studies (53–56), the number of mice needed for each experiment was determined. Kaplan–Meier method was used to estimate survival as a function of time (days after implantation), and a two-sided log-rank test was performed to test the statistical significance of the difference between the different groups. P values less than .05 were considered statistically significant.

In all analysis, means and outcome variables are given as point estimates with 95% confidence intervals (CIs). Mean and interquartile range are shown in the scatter diagram of subcutaneously xenografted tumor size.

All statistical analyses were performed using Office Excel 2004 (Microsoft Corporation, Redmond, WA) or SPSS software (version 11.5; SPSS, Inc, Chicago, IL).

Results

Analysis of TRPC6 and TRPC3 Expression in Human Glioma

To study the role of TRPC6 and TRPC3 channels in human glioma, we first examined their protein expression in clinical glioma samples. Representative immunoblots were shown in Figure 1, A. Analysis of the band densities revealed that in 54% of the glioma samples, TRPC6 was expressed (mean = 3.67, 95% CI = 2.84 to 4.5, $P < .001$ vs normal tissues) at approximately threefold higher levels than in normal tissues (mean = 1.09, 95% CI = 0.64 to 1.54) (Figure 1, B). There was no difference in the mean level of expression of TRPC3 between the glioma samples (mean = 1.69, 95% CI = 1.21 to 2.17, $P = .27$ vs normal tissues) and the normal tissues (mean = 2.20, 95% CI = 1.32 to 3.08) (Figure 1, C).

Next, we assessed the expression and distribution of TRPC6 in normal and glioma tissues for both protein and mRNA levels. Immunohistological staining of the tissues using a polyclonal TRPC6 antibody showed strong staining in the GBM samples (Figure 1, D, a–i). Normal glial (para-tumor) tissues that are non-neuronal exhibited little immunostaining, but strong signals were noted in the pyramid-shaped neurons (Figure 1, D, p–r). Also, as shown in Supplementary Figure 3 (available online), TRPC6 staining of neurons (NeuN positive) was strong, whereas there was no signal in the normal glial cells (NeuN negative). In contrast, tumor tissues (glioma) that were NeuN negative showed strong TRPC6 staining. These results suggested that TRPC6 was predominantly expressed in the neurons and in the glioma cells. In astrocytoma (grade 2 glioma) and anaplastic oligodendrocytoma (grade 3 glioma) samples (Figure 1, D, j–o), the cells had weaker immunostaining for TRPC6, compared with GBM samples (Figure 1, D, a–i). Immunohistological staining of grade 1 glioma is not shown.

The relative expression levels of different grades of glioma are shown in a bar chart (Figure 1, E). In low-grade (grades 1 and 2) glioma sections, none (zero of eight), 37.5% (three of eight), and 62.5% (five of eight) of the samples showed strong, moderate, or weak staining, respectively. In grade 3 glioma sections, none (zero of seven), 71.4% (five of seven), and 28.6% (two of seven) of the samples showed strong, moderate, or weak staining,

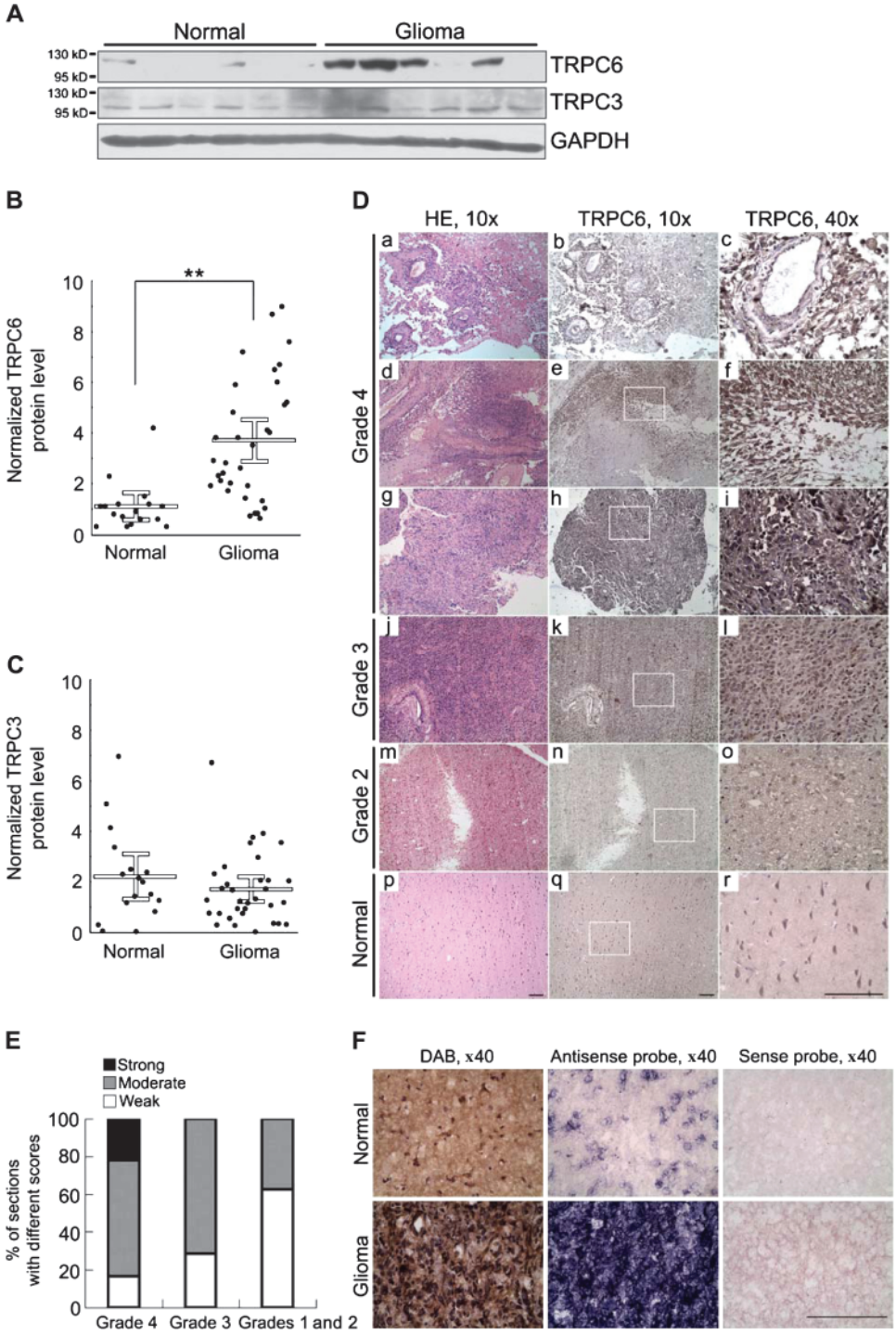

Figure 1. Expression of TRPC6 protein in human glioma tissue. **A**) Representative immunoblots of total lysates extracted from human glioma (six samples shown) and normal brain (six samples shown) tissues probed with anti–transient receptor potential canonical (TRPC)6 (106 kDa) or anti-TRPC3 (97 kDa) antibodies. GAPDH served as the protein loading control. **B** and **C**) Quantification of TRPC6 and TRPC3 protein levels in glioma (n = 33) and normal brain (n = 17) tissues from the immunoblots. Each **dot** represents the band density of TRPC6 and 3 proteins normalized to that of the corresponding GAPDH in each sample. n = number of samples. Means and 95% confidence intervals are represented by **open lines** and **error bars**. $^{**}P < .001$ vs normal, calculated using the two-sided Student *t* test. **D**) Representative immunohistological staining samples of human glioma or normal brain tissues with anti-TRPC6 antibody. **a–i**) Three glioblastoma multiforme (GBM, grade 4) samples; **j–l**) anaplastic oligodendrocytoma (grade 3 oligodendrocytoma); **m–o**) grade 2 astrocytoma; and **p–r**) normal (para-tumor) tissues. Sections were stained by the 3,3′-diaminobenzidine (DAB) staining method to detect TRPC6 protein in the tissues and were counterstained with hematoxylin to stain the nucleus. Serial sections of the same samples were used for hematoxylin and eosin (HE) staining. Magnified ×40 panels represented the **white rectangles** in the ×10 panels. Scale bar = 100 μm. **E**) **Bar graph** representation of TRPC6 immunohistological scores in glioma of different grades. The percentage of sections with different scores (strong, moderate, and weak) in each grade is shown. Grade 4 glioma (GBM), n = 18; grade 3, n = 7; grades 1 and 2 combined, n = 8. n = number of samples. **F**) Expression of TRPC6 mRNA in glioma and normal tissues detected by in situ hybridization. Immunostaining by anti-TRPC6 antibody (DAB, ×40) on serial sections of the same samples used for immunohistological staining. Sense probe (×40) was used as a negative control, and the antisense probe (×40) was used to detect the TRPC6 mRNA. Scale bar = 100 μm.

respectively. In grade 4 GBM sections, 22.2% (four of 18), 61.1% (11 of 18), and 16.7% (three of 18) of the samples showed strong, moderate, or weak staining, respectively. These results implied that the expression level of TRPC6 was associated with the glioma malignancy grades.

We then performed in situ hybridization to examine the mRNA level of TRPC6 in normal and glioma tissues. Hybridization of a TRPC6-specific antisense probe was detected in glioma cells, but not in normal tissues, whereas hybridization of a sense probe was negative in these sections (Figure 1, F). In the serial sections of the same tumor samples, expression of TRPC6 protein was detected by immunostaining (Figure 1, F).

Collectively, these results suggested that TRPC6 expression, at both protein and mRNA levels, was increased in human glioma. The increased expression was also associated with the glioma malignancy grades.

Activation of TRPC6 Channels in Glioma Cells

We next studied whether TRPC6 channels were functional and could mediate Ca^{2+} influx in glioma cells. It is known that PDGF

receptors are commonly expressed in glioma cells (32,57) and PDGF can activate phospholipase C (32), a key molecule for the activation of TRPC6 (28). Fura-2 AM imaging of Ca^{2+} activity showed that PDGF induced an elevation of intracellular Ca^{2+} concentration $[Ca^{2+}]_i$ in U87 glioma cells. This elevation was attenuated by a putative TRPC channel blocker, SKF96365 (58,59), or by expressing the dominant-negative form of TRPC6 (DNC6), or small interfering RNA against TRPC6 in U87 cells by 33%, 50%, and 64%, respectively (Figure 2, A–D, and Supplementary Figure 4, A–C, available online). These results indicated that TRPC6 channels partially mediated PDGF-induced $[Ca^{2+}]_i$ elevation in U87 cells.

Next, we incubated U87 cells in a Ca^{2+}-free extracellular solution, in which the resting level of $[Ca^{2+}]_i$ did not change (Supplementary Figure 4, D, available online). We found that PDGF still induced $[Ca^{2+}]_i$ elevation, although the magnitude was smaller than that in extracellular solution containing Ca^{2+}, indicating that PDGF-induced $[Ca^{2+}]_i$ elevation was because of both intracellular Ca^{2+} release and extracellular Ca^{2+} entry (Figure 2, E and F). Indeed, PDGF has been reported to induce both Ca^{2+} release and Ca^{2+} entry in human glioma cells (60). On addition of Ca^{2+}, PDGF again induced $[Ca^{2+}]_i$ elevation similar to that found in the cells incubated in the presence of Ca^{2+}. Importantly, DNC6 markedly inhibited this $[Ca^{2+}]_i$ elevation (Figure 2, E and F). Moreover, the PDGF-induced $[Ca^{2+}]_i$ elevation was abolished by treatment with 2-aminoethyl diphenylborate, an IP_3 receptor antagonist (61) (Supplementary Figure 4, E, available online). Therefore, it was likely that PDGF stimulated Ca^{2+} release through the IP_3 receptor to induce extracellular Ca^{2+} entry because PDGF can enhance store-operated Ca^{2+} entry (62)—an extracellular Ca^{2+} entry in response to Ca^{2+} release from internal stores (29). This notion was supported by the findings that the $[Ca^{2+}]_i$ elevation induced by depleting internal Ca^{2+} stores using cyclopiazonic acid, a Ca^{2+}-ATPase inhibitor known to deplete internal stores (45), was markedly reduced by DNC6 (Figure 2, G and H). Together, these results suggested that functional TRPC6 channels were present in the glioma cells, and internal Ca^{2+} release triggered by PDGF was followed by a store-operated Ca^{2+} entry through the TRPC6 channels.

Effect of Inhibition of TRPC6 Activity or Expression on Glioma Cell Growth

Because TRPC6 was Ca^{2+} permeable in glioma cells and Ca^{2+} is important for cell proliferation, we next tested whether TRPC6 has a role in glioma cell proliferation. First, we checked the expression levels of TRPC6 protein and mRNA in three human glioma cell lines (U251, U87, and T98G) and in one rat glioma cell line (C6) (Supplementary Figure 5, A and B, available online). To examine whether inhibition of TRPC6 activity has an effect on glioma cell growth, the two putative inhibitors of TRPC activity, SKF96365 and 2-aminoethyl diphenylborate, were tested on U251 and C6 cells. In C6 cells, a dose-dependent inhibition of growth was observed with SKF96365, and after 48 hours, at 20 μM concentration, there was an approximately 50% inhibition of growth (Supplementary Figure 6, A and B, available online). In U251 cells, a dose-dependent inhibition of growth was observed with 2-aminoethyl diphenylborate, and after 48 hours, at 300 μM concentration, there was an approximately 60% inhibition of growth (Supplementary Figure 6, C, available online). In C6 cells, at 100 μM concentration of 2-aminoethyl diphenylborate, there was an approximately 50% inhibition of growth (Supplementary Figure 6, D, available online). These results indicated that inhibition of TRPCs suppressed the growth of glioma cells.

The TRPC inhibitors used in the cell growth analysis were not specific to TRPC6 channels. Therefore, we wanted to exclude the possibility of nonspecific effects of these inhibitors (63). To establish the specific inhibitory effect of DNC6 on TRPC6 activity, we showed that DNC6 expression blocked the TRPC6 channel–mediated current (Supplementary Figure 7, A–E, available online). Glioma cells (U251, U87, and T98G) were infected with adenovirus-expressing DNC6 or wild-type TRPC6 (WTC6), and infection efficiencies were estimated as shown in Supplementary Figure 2, available online. Analysis by qPCR showed that infection with DNC6 resulted in a 6.4-fold increase in TRPC6 protein level (Supplementary Figure 8, A, available online) but did not affect the expression of TRPC1 (mean = 1.93, 95% CI = 0.93 to 2.93, $P = .21$ vs GFP) and TRPC3 (mean = 1.30, 95% CI = 0.78 to 1.82, $P = .37$ vs GFP)—the two members of TRPC subfamily found in these glioma cells (Supplementary Figures 5, A, and 8, A, available online).

Cell growth analysis showed that the number of U251 and U87 cells infected with DNC6-expressing adenovirus was markedly reduced compared with that of the cells infected with GFP- or WTC6-expressing adenovirus (Figure 3, A and B). In colony formation assays, GFP fluorescence was observed in the cells after 14 days indicating the length of time for the expression of the transfected genes. Infection with DNC6 markedly inhibited the clonogenic ability of both U251 and U87 cells as reflected by the size and number of colonies (Figure 3, C). In U251 cells, the normalized OD_{595} value of DNC6-infected colonies was 0.10 (95% CI = 0.056 to 0.15, $P < .001$ vs GFP or WTC6) and in WTC6-infected colonies was 1.03 (95% CI = 0.94 to 1.13, $P = .5$ vs GFP), respectively. Similarly, DNC6 infection showed a substantially decreased OD_{595} value of the colonies in U87 cells (Figure 3, D). Because infection with WTC6 did not affect cell growth, it was unlikely that the inhibitory effect of DNC6 was because of the cytotoxic effect of overexpressing a large protein. These results suggested that blockade of TRPC6 channels inhibited growth in U251 and U87 cells.

To rule out the possibility that the observed effect of TRPC6 on glioma cell growth may have been caused by nonspecific blockade of TRPC channels by DNC6 (50), we infected U251 cells with lentivirus-based shRNAs to knock down the expression of TRPC6. Scrambled shRNA based on shTRPC6-1 was used as a control. The TRPC6 protein level was markedly reduced by shTRPC6-1 (C6-1) (mean = 0.41, 95% CI = 0.18 to 0.64, $P = .03$ vs control) and shTRPC6-2 (C6-2) (mean = 0.36, 95% CI = 0.31 to 0.41, $P = .001$ vs control). The mRNA levels of TRPC1 and TRPC3 remained unaffected on infection with C6-1 (for TRPC1, mean = 1.01, 95% CI = 0.87 to 1.15, $P = .45$ vs control; for TRPC3, mean = 0.89, 95% CI = 0.67 to 1.11, $P = .28$ vs control) and C6-2 (for TRPC1, mean = 0.89, 95% CI = 0.48 to 1.3, $P = .63$ vs control; for TRPC3, mean = 1.03, 95% CI = 0.59 to 1.47, $P = .35$ vs control) (Supplementary Figure 8, B, available online). In colony formation

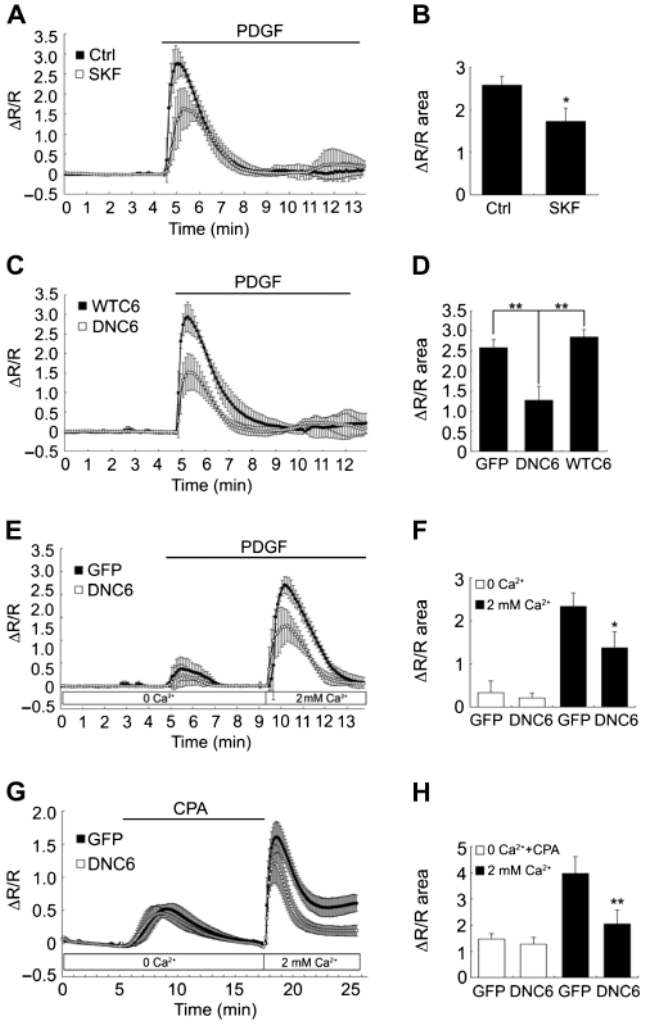

Figure 2. Functional activity of transient receptor potential canonical 6 (TRPC6) channels in glioma cells. Fura-2 AM imaging showing induction and attenuation of transient elevation of $[Ca^{2+}]_i$ in U87 cells. R refers to the ratio of the emission at 500 nm induced by 340 and 380 nm excitation, captured at 6-second intervals. ΔR/R was calculated as $(R - R_{baseline})/R_{baseline}$, $R_{baseline}$ being the mean value of R during pretreatment. The recording time in minutes is shown. **Squares** represent the mean values. **Error bars** = 95% confidence intervals. Corresponding **bar charts** show the area of ΔR/R curve in the Fura-2 AM imaging, 3 minutes after addition of platelet-derived growth factor-BB (PDGF-BB) or 10 minutes after addition of cyclopiazonic acid (CPA). In all **bar charts**, the *y*-axis shows the absolute value of the area divided by 100. Means and upper 95% confidence intervals are shown. All *P* values were calculated using the two-sided Student *t* test. Ctrl = control; n = number of cells. **A**) Induction with 50 ng/mL PDGF-BB (Ctrl, **solid square**) and attenuation with 20 μM SKF96365 (SKF, **open square**). Medium was supplemented with calcium (Ca^{2+}). **B**) **Bar chart** corresponds to (**A**). Ctrl, n = 48; SKF, n = 32. **P* = .014 vs Ctrl. Data from three independent experiments are shown in (**A**) and (**B**). **C**) Induction with PDGF-BB in cells infected with adenovirus-expressing wild-type TRPC6 (WTC6, **solid square**) and attenuation in cells expressing the dominant-negative form of TRPC6 (DNC6, **open square**). Duration of infection was 48 hours. Medium was supplemented with Ca^{2+}. **D**) **Bar chart** corresponds to (**C**). Cells infected with adenovirus expressing green fluorescent protein (GFP) served as the control. GFP, n = 48; DNC6, n = 51; WTC6, n = 45. ***P* = .001, GFP vs DNC6, and ***P* < .001, WTC6 vs DNC6. Data from at least three independent experiments are shown in (**C**) and (**D**). **E**) Induction with PDGF-BB in cells infected with GFP (**solid square**) or DNC6 (**open square**) in Ca^{2+}-free medium (0 Ca^{2+}) and Ca^{2+}-containing medium (2 mM Ca^{2+}). **Smaller peaks** represent the internal Ca^{2+} release induced by PDGF-BB, and **larger peaks** represent the extracellular Ca^{2+} entry on addition of 2 mM Ca^{2+} after about 9–10 minutes. **F**) **Bar chart** corresponds to (**E**). Induction with PDGF-BB in medium without (**open bar**) or with (**solid bar**) Ca^{2+}. GFP, n = 36; DNC6, n = 34. **P* = .011 vs GFP. Data from at least three independent experiments are shown in (**E**) and (**F**). **G**) Induction with 10 μM CPA in cells infected with GFP (**solid square**) or DNC6 (**open square**) in Ca^{2+}-free medium (0 Ca^{2+}). **Smaller peaks** represent the internal Ca^{2+} release. After the $[Ca^{2+}]_i$ returned to the baseline, 2 mM Ca^{2+} (2 mM Ca^{2+}) was added to the medium and a transient elevation of $[Ca^{2+}]_i$ was again induced, represented by the **larger peaks**. **H**) **Bar chart** corresponds to (**F**). Induction with CPA in medium without (**open bar**) or with (**solid bar**) Ca^{2+}, 10 minutes after addition of CPA (**open bar**) or 8 minutes after addition of Ca^{2+} (**solid bar**). GFP, n = 90; DNC6, n = 107. ***P* = .004 vs GFP. Data from four independent experiments are shown in (**G**) and (**H**).

assays, the colony size and number in the control group clearly exceeded those in C6-1 and C6-2 groups (Figure 3, E and F). The normalized OD_{595} in C6-1 and C6-2 was 0.57 (95% CI = 0.31 to 0.83, *P* = .032 vs control) and 0.25 (95% CI = 0.21 to 0.29, *P* < .001 vs control), respectively (Figure 3, G). Together, these results suggested that specific inhibition of TRPC6 channels suppressed glioma cell growth.

Effect of Inhibition of TRPC6 Activity or Expression on G2 Phase Progression of Glioma Cells

TRPC6 is a Ca^{2+}-permeable channel in glioma cells, and Ca^{2+} ions are important for cell cycle regulation (11). To elucidate the mechanism by which inhibition of TRPC6 suppressed glioma cell growth, we first investigated the effect of inhibition on cell cycle. U251 cells were assayed by flow cytometry to determine the cell cycle profiles after infection with adenovirus expressing GFP, DNC6, or WTC6 or infection with lentivirus-based shRNA constructs (Figure 4, A and B). The percentage of cells at G2/M phase in GFP-infected cells was 24.6% (95% CI = 20.2% to 29.0%, *P* = .005 vs DNC6), in DNC6-infected cells was 38.8% (95% CI = 33.9% to 43.7%), and in WTC6-infected cells was 24.2% (95% CI = 19.5% to 28.9%, *P* = .005 vs DNC6), respectively.

The percentage of cells at G2/M phase in control (scrambled shRNA) was 18.3% (95% CI = 16.6% to 20.0%), in C6-1 (shTRPC6-1) was 30.1% (95% CI = 28.7% to 31.5%, *P* < .001 vs control), and in C6-2 (shTRPC6-2) was 28.6% (95% CI = 26.7% to 30.5%, *P* < .001 vs control), respectively (Supplementary Table 2, available online). These results suggested that blockade of TRPC6 channels arrested glioma cells at the G2/M phase of the cell cycle. In both DNC6-infected (GFP, mean = 0.99%, 95% CI = 0.17% to 1.81%, *P* = .01 vs DNC6; DNC6, mean = 3.02%, 95% CI = 2.69% to 3.35%; and WTC6, mean = 1.29%, 95% CI = 0.87% to 1.71%, *P* < .001 vs DNC6) and shTRPC6-infected (control, mean = 0.95%, 95% CI = 0.38% to 1.52%; C6-1, mean = 1.61%, 95% CI = 1.00% to 2.22%, *P* = .18 vs control; C6-2, mean = 4.03%, 95% CI = 3.04% to 5.02%, *P* < .001 vs control) groups, the percentage of apoptotic cells (subG0 cells) was marginally increased, likely because of prolonged G2/M phase arrest (Supplementary Table 2, available online).

The T-type VGCCs are known to be involved in tumor cell growth (16,64). The α1G subunit of T-type VGCCs (CACNA1G) was expressed by U251 cells (Supplementary Figure 9, A, available online), so we tested if mibefradil, a putative inhibitor for T-type VGCCs, has an effect on U251 cell proliferation. Approximately

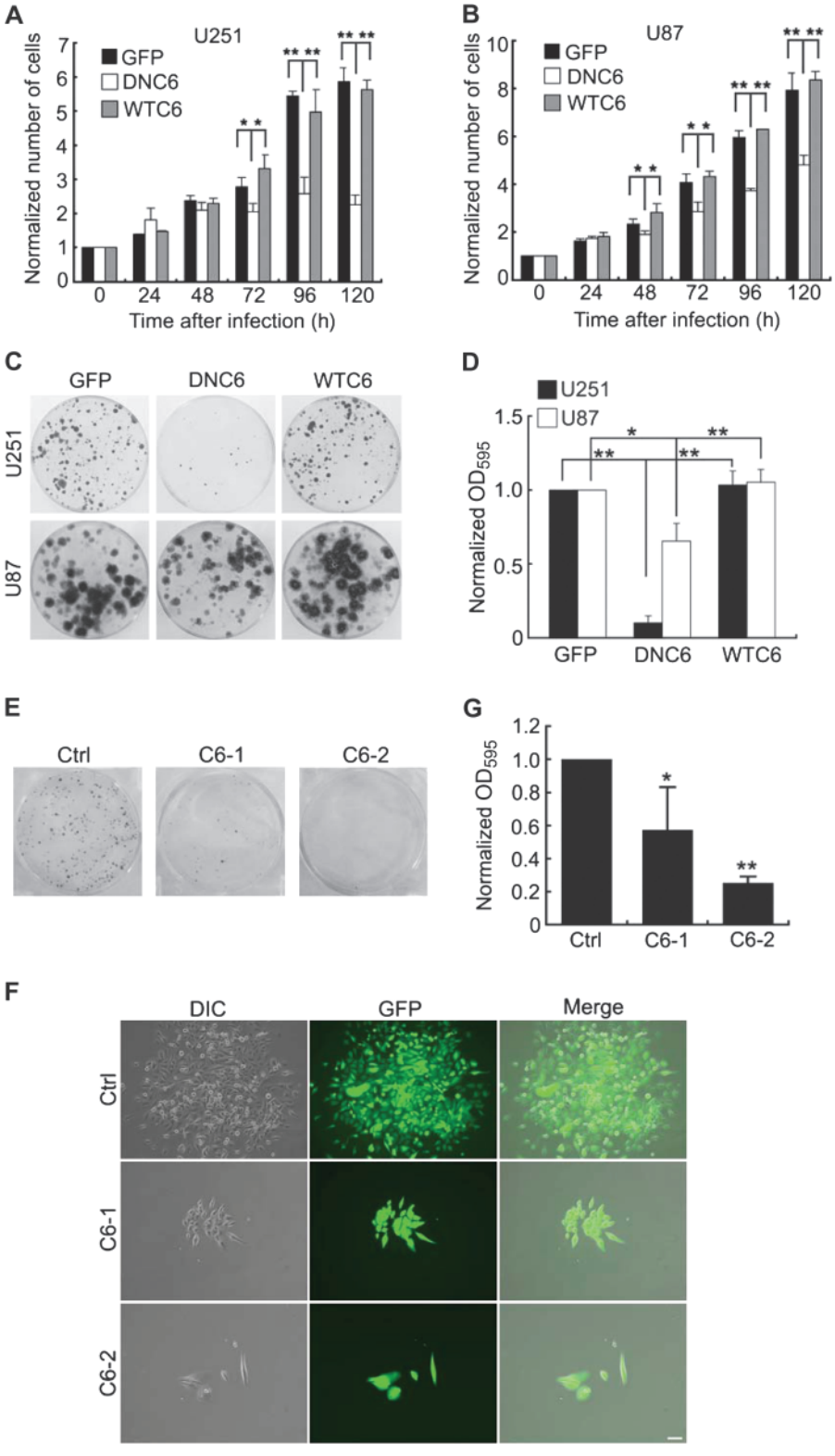

Figure 3. Effect of inhibition of transient receptor potential canonical 6 (TRPC6) activity or expression on glioma cell growth. **A** and **B**) Number of U251 and U87 cells infected with adenovirus expressing green fluorescent protein (GFP), DNC6, or WTC6. Cell numbers were normalized to those at day 0. Means and upper 95% confidence intervals from three independent experiments performed in duplicate are shown. **P* < .05, ***P* < .01, GFP or WTC6 vs DNC6. **C**) Representative images of U251 and U87 colonies infected with adenovirus expressing GFP, DNC6, or WTC6. Colonies stained with crystal violet after 14 days of seeding are shown. **D**) Quantification of U251 and U87 colonies (shown in **C**) by measuring the optical density at 595 nm (OD_{595}). OD_{595} values of DNC6 and WTC6 groups were normalized to that of GFP group. Means and upper 95% confidence intervals are shown. Data are representative of four independent experiments, performed in duplicate. **P* < .05, ***P* < .01, GFP or WTC6 vs DNC6. **E**) U251 colonies infected with lentivirus-based scrambled short hairpin RNA (shRNA) (Ctrl), shTRPC6-1 (C6-1), and shTRPC6-2 (C6-2). Colonies stained with crystal violet after 14 days of seeding were shown. Ctrl = control. **F**) Differential interference contrast (DIC) and fluorescent (GFP) images of typical single colonies formed by U251 cells infected with the indicated lentiviral constructs—scrambled shRNA (Ctrl), shTRPC6-1 (C6-1), and shTRPC6-2 (C6-2). The duration of infection was 72 hours before seeding. The lentivirus was GFP tagged. Ctrl = control. Images were taken 14 days after seeding. Scale bar = 100 μm. Merge panels show the merged DIC and GFP images. **G**) Quantification of the U251 colonies (shown in **E**) by measuring the OD_{595}. Means and upper 95% confidence intervals are shown. Data are representative of four independent experiments performed in duplicate. **P* = .032, ***P* < .001 vs Ctrl. All *P* values were calculated using the two-sided Student *t* test.

40% inhibition of cell proliferation was observed with both mibefradil and SKF96365 (Supplementary Figure 9, B, available online). However, unlike SKF96365, mibefradil did not affect the G2/M phase transition (Supplementary Figure 9, C, and Table 2, available online). Furthermore, knockdown of CACNA1G expression by shRNA did not influence G2/M phase transition (Figure 4, C and D). However, both mibefradil and shRNA targeted to CACNA1G caused S phase arrest (control, mean = 11.9%, 95% CI = 11.1% to 12.7%; mibefradil, mean = 13.5%, 95% CI = 12.7% to 14.3%, *P* = .03 vs control; control RNA interference, mean = 9.38%, 95% CI = 7.66% to 11.1%; CACNA1G RNA interference, mean = 19.1%, 95% CI = 14.8% to 23.4%, *P* = .005 vs control RNA interference;

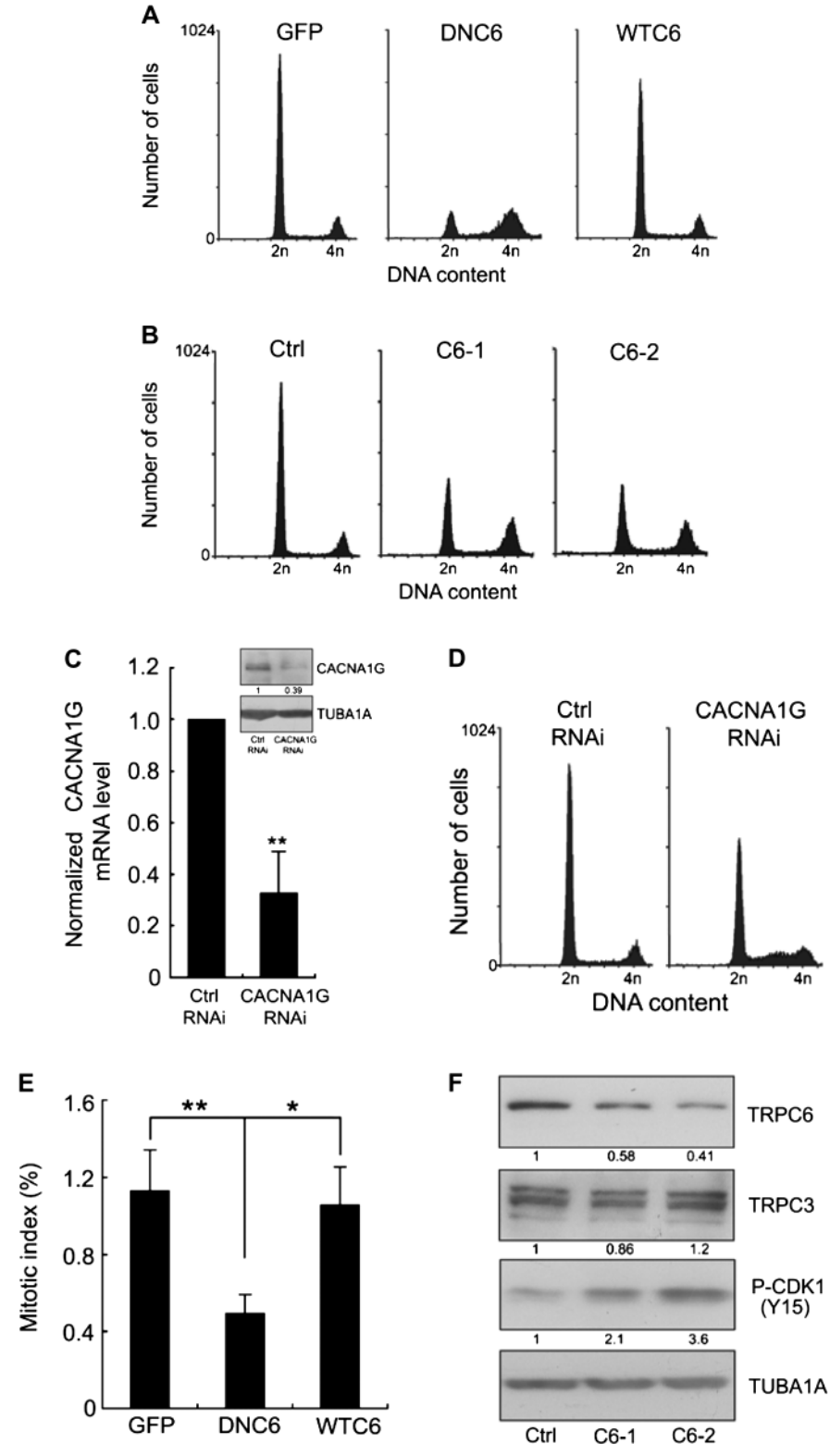

Figure 4. Effect of inhibition of transient receptor potential canonical 6 (TRPC6) activity or expression on G2 phase arrest. **A** and **B**) Flow cytometric analysis of U251 DNA content after infection with adenovirus expressing green fluorescent protein (GFP), DNC6, and WTC6 for 72 hours or the indicated lentivirus-based short hairpin RNA (shRNA) constructs (Ctrl, C6-1, and C6-2), 5–10 days after infection. DNA content is shown as 2n and 4n in the *x*-axis. 2n = cells in G0/G1 phase, and 4n = cells in the G2/M phase. Data are representative of four independent experiments. Ctrl = control, scrambled shRNA (Ctrl); C6-1 = shTRPC6-1 and C6-2 = shTRPC6-2. **C**) Quantitative real-time polymerase chain reaction and immunoblot analysis (inset) showing knockdown of CACNA1G in U251 cells by lentivirus-based shRNA constructs against the CACNA1G (CACNA1G RNA interference [RNAi]). Control (Ctrl) RNAi was nonsense shRNA. Data are representative of five independent experiments. TUBA1A served as the protein loading control. **Error bar** = upper 95% confidence interval. $**P < .001$ vs Ctrl RNAi. **D**) Flow cytometric analysis of U251 cell cycle after infection with the lentivirus-based shRNA construct (CACNA1G RNAi) (shown in **C**), 5–10 days after infection. Data shown are a representative of six independent experiments. **E**) Mitotic index of U251 cells after infection with adenovirus expressing GFP, DNC6, and WTC6 for 72 hours. Mitotic index (%) is the percentage of mitotic cells in total cells. Means and upper 95% confidence interval from three independent experiments are shown. $**P = .005$, GFP vs DNC6, and $*P = .022$, WTC6 vs DNC6. **F**) Effect of TRPC6 knockdown on the level of phosphorylated cyclin-dependent kinase 1 at tyrosine15 (P-CDK1 [Y15]). Immunoblot analysis of total U251 cell lysates using the indicated antibodies. Proteins were extracted approximately 10 days after infection. C6-1 and -2 lanes show approximately 40% and 60% decrease in TRPC6 level and increased in P-CDK1 (Y15) level by two- or four-fold, respectively. TRPC3 blots show that TRPC6 knockdown did not have an effect on its homolog. TUBA1A served as the protein loading control. Data are representative of three independent experiments. All *P* values were calculated using the two-sided Student *t* test.

Supplementary Table 2, available online). These results suggested that in U251 cells, Ca^{2+} influx through TRPC6 channels, but not T-type VGCCs, was critical for G2/M phase progression.

To further explore the effect of inhibition of TRPC6 channels on cell cycle, we determined the mitotic index of U251 cells infected with adenovirus expressing GFP, DNC6, and WTC6 (Supplementary Figure 10, available online). Mitotic index of GFP-infected cells was 1.13% (95% CI = 0.92% to 1.34%), DNC6-infected cells was 0.49% (95% CI = 0.39% to 0.59%, $P = .005$ vs GFP, $P = .022$ vs WTC6), and WTC6-infected cells was

1.05% (95% CI = 0.83% to 1.27%), respectively (Figure 4, E), indicating that substantially fewer cells were present in the M phase on inhibition of TRPC6 channel. Collectively, these results suggested that blocking TRPC6 channels in glioma cells resulted in cell cycle arrest in the G2 phase.

The CDK1 and CCNB1 (also known as cyclin B1) complex is the central regulator of G2/M phase, and dephosphorylation at tyrosine15 and threonine14 of CDK1 is critical for its activation and G2/M phase transition (65). Knockdown of TRPC6 expression in U251 cells increased the level of phosphorylated CDK1 at the tyrosine15 residue (Figure 4, F). Similarly, in T98G cells, expression of DNC6 enhanced the level of phosphorylated CDK1 at the tyrosine15 residue (data not shown). Together, these results suggested that inhibition of TRPC6 induced G2 phase arrest in glioma cells, and Ca^{2+} influx through TRPC6 channels was essential for CDK1 activation and G2/M phase transition of the cell cycle.

Effect of Inhibition of TRPC6 Activity or Expression on CDC25C Expression

The CDC25C phosphatase is a critical component in the G2/M phase transition because it activates CDK1 via dephosphorylation at the tyrosine15 and threonine14 residues (39). We first examined whether blockade of TRPC6 activity affected CDC25C expression. CDC25C protein levels were substantially reduced in both U251 and T98G cells after DNC6 infection (Figure 5, A, and Supplementary Figure 11, A, available online), and this reduction was noted within 24 hours of infection (Figure 5, B). CDC25A or CDC25B protein levels were either not affected or mildly affected (Figure 5, A, and Supplementary Figure 11, A, available online). Knockdown of TRPC6 expression with shRNA also decreased the protein levels of CDC25C but not of CDC25A or CDC25B (Figure 5, C).

Analysis by qPCR revealed that normalized CDC25C mRNA levels were reduced to 0.37 (95% CI = 0.22 to 0.52, $P < .001$ vs GFP or WTC6) in U251 cells and 0.36 (95% CI = 0.19 to 0.53, $P = .002$ vs GFP, $P = .003$ vs WTC6) in T98G cells, respectively, after adenovirus-based DNC6 infection (Figure 5, D). Similarly, normalized CDC25C mRNA levels were reduced to 0.68 (95% CI = 0.54 to 0.82, $P = .004$ vs control) in U251 cells infected with lentivirus-based shTRPC6-1 (C6-1) and 0.54 (95% CI = 0.37 to 0.71, $P = .01$ vs control) in cells infected with shTRPC6-2 (C6-2) (Figure 5, E). The reverse transcription–polymerase chain reaction analysis further confirmed that DNC6 expression did not affect CDC25A or CDC25B mRNA levels but decreased the level of CDC25C mRNA 24 hours after infection (Supplementary Figure 11, B and C). These results suggested that reduction of CDC25C expression as a result of inhibition of TRPC6 activity or expression occurred before the G2/M phase arrest and that TRPC6 proteins were essential for CDC25C expression.

To determine whether Ca^{2+} influx through TRPC6 channels was essential for CDC25C expression, we incubated U251 cells in a Ca^{2+}-free medium and found that protein levels of CDC25C, but not of CDC25A or CDC25B, were markedly reduced (Supplementary Figure 11, D, available online). However, inhibition of T-type VGCCs did not affect CDC25C protein levels (Figure 5, F, and Supplementary Figure 11, E, available online). These results implied that Ca^{2+} influx through TRPC6 channels, rather than through T-type VGCCs, was important for CDC25C expression, and the differential effect of TRPC6 and T-type VGCCs on CDC25C expression may contribute to their different roles in the cell cycle. Furthermore, overexpression of CDC25C reversed the DNC6-induced increase in the level of phosphorylated CDK1 at tyrosine15 (Figure 5, G). These results suggested that blockade of TRPC6 channels inhibited CDK1 activation via suppression of CDC25C expression.

Effect of Inhibition of TRPC6 Activity on Radiosensitization of Glioma Cells

The above results showed that inhibition of TRPC6 activity induced glioma cell cycle arrest at G2/M phase, the phase most sensitive to irradiation (66,67). Therefore, we examined whether TRPC6 inhibition enhanced the antiproliferative effect of ionizing radiation on glioma cells. At 2 and 4 Gy of irradiation, the surviving fraction of U251 cells treated with SKF96365 group was greatly reduced compared with vehicle control group ($P = .006$ at 2 Gy and $P = .005$ at 4 Gy vs vehicle control) (Figure 6, A and B). The surviving fraction of cells was calculated by normalizing the OD_{595} of the colonies, for each dose of irradiation, to that of the corresponding nonirradiated colonies. Similarly, the survival in U251 cells infected with adenovirus-based DNC6 was markedly reduced compared with the vehicle control ($P < .001$ at 2 Gy and $P = .002$ at 4 Gy vs GFP) (Figure 6, C). These results suggested that inhibition of TRPC6 activity enhanced the antiproliferative effect of irradiation in glioma cells.

Effect of Inhibition of TRPC6 Activity on the Development of Xenografted Human Glioma

To provide evidence that TRPC6 channels are indeed important for glioma development in vivo, we established both subcutaneously and intracranially xenografted glioma models in nude mice.

In the subcutaneous model, after implantation, tumor volumes were estimated every 5 days (Figure 7, A). DNC6-infected cells grew statistically significantly slower than GFP- or WTC6-infected cells. Thirty days after implantation, the mice bearing tumors did not show deterioration in physiological conditions, and tumors formed by DNC6-infected cells were visibly smaller than those formed by GFP- or WTC6-infected cells (Figure 7, B). The mean tumor volume of GFP-infected cells was 342.5 mm^3 (interquartile range = 204.2–465.5 mm^3, n = 7), of DNC6-infected cells was 55.8 mm^3 (interquartile range = 43.5–65.6 mm^3, n = 7, $P = .014$ vs GFP, $P < .001$ vs WTC6), and of WTC6-infected cells was 352.0 mm^3 (interquartile range = 276.8–404.5 mm^3, n = 7) (Figure 7, C), respectively.

In the intracranial model (Figure 7, D), mice (n = 15) bearing glioma originating from DNC6-infected U87 cells had longer survival time (mean = 37.5 days, 95% CI = 35.8 to 39.2 days, $P < .001$ vs GFP or WTC6) compared with mice bearing glioma from GFP-infected (mean = 27.7 days, 95% CI = 26.5 to 28.8 days) or WTC6-infected (mean = 28.2 days, 95% CI = 26.9 to 29.5 days) cells (n = 13 in each group). After 20 days of implantation, the staining of coronal sections of the brains with hematoxylin and eosin showed that tumors from DNC6-infected

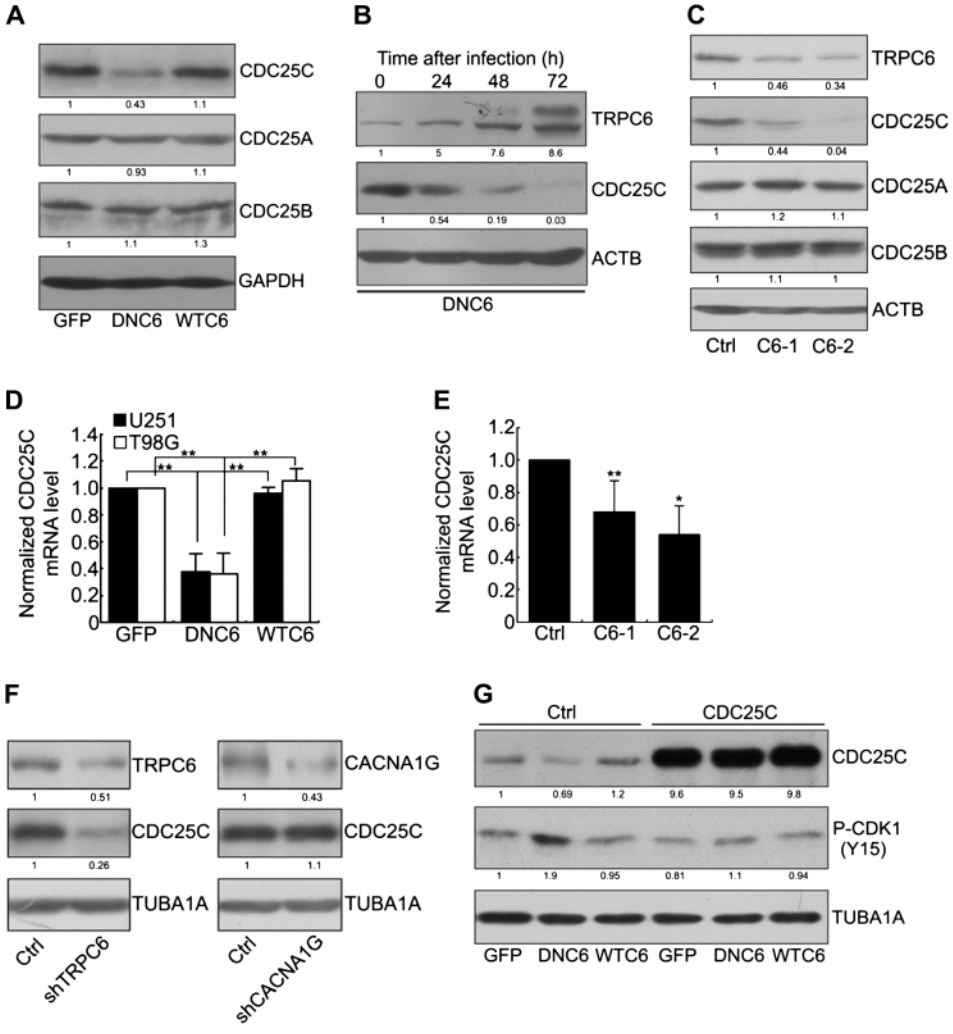

Figure 5. Effect of inhibition of transient receptor potential canonical 6 (TRPC6) activity or expression on cell division cycle 25 homolog C (CDC25C) expression. **A**) U251 cells were infected with adenovirus expressing green fluorescent protein (GFP), DNC6, and WTC6 for 72 hours and analyzed for CDC25C, CDC25A, and CDC25B by immunoblotting. GAPDH served as the protein loading control. One representative blot of three independent experiments is shown. **B**) Time-dependent decrease in CDC25C expression after adenovirus-based DNC6 expression in U251 cells. Cell lysates were analyzed for TRPC6 and CDC25C expression by immunoblotting. ACTB served as the protein loading control. One representative blot of three independent experiments was shown. **C**) U251 cells were infected with lentiviral-based scrambled short hairpin RNA (Ctrl), shTRPC6 (C6-1 and C6-2) for 120 hours and analyzed for TRPC6, CDC25C, CDC25A, and CDC25B by immunoblotting. ACTB served as the protein loading control. One representative blot of three independent experiments is shown. **D**) Quantitative real-time polymerase chain reaction (qPCR) results showing reduction in CDC25C mRNA levels 72 hours (U251 cells) or 96 hours (T98G cells) after adenovirus-based DNC6 infection. CDC25C mRNA levels were normalized to those in GFP infection. Means and upper 95% confidence intervals from three independent experiments are shown. $^{**}P < .001$, GFP or WTC6 vs DNC6 in U251 cells; $^{**}P = .002$, GFP vs DNC6, $^{**}P = .003$, WTC6 vs DNC6 in T98G cells. **E**) qPCR results showing reduction in CDC25C mRNA levels in U251 cells 120 hours after lentivirus-based infection with scrambled shRNA (Ctrl) and shTRPC6 (C6-1 and C6-2). CDC25C mRNA levels were normalized to those in the control group. Ctrl = control. Means and upper 95% confidence intervals from three independent experiments are shown. $^{*}P = .01$, C6-2 vs Ctrl; $^{**}P = .004$ C6-1 vs Ctrl. **F**) U251 cells were infected with lentivirus-based shTRPC6 (C6-2 was used) or lentivirus-based shCACNA1G for 120 hours and analyzed for TRPC6, CACNA1G, and CDC25C by immunoblotting. TUBA1A served as the protein loading control. Data are representative of three independent experiments. **G**) Effect of CDC25C overexpression on P-CDK1 (Y15) level in T98G cells 24 hours before DNC6 infection. TUBA1A served as the protein loading control. Data are representative of two independent experiments. All *P* values were calculated using the two-sided Student *t* test.

cells were visibly smaller than those from GFP- or WTC6-infected cells (Figure 7, E).

These results suggested that TRPC6 channel activity was important for glioma development.

Discussion

In this study, we showed that TRPC6 channels, which are permeable to Ca^{2+}, contributed to glioma development via regulating the G2 phase progression. Several lines of evidence supported this conclusion. First, we observed that TRPC6 was highly expressed in human glioma and level of expression was associated with grade. Second, we showed that TRPC6 channels in glioma cells were Ca^{2+} permeable and could be activated by PDGF. Third, inhibition of TRPC6 expression suppressed glioma growth both in vitro and in vivo. Fourth, inhibition of TRPC6 expression induced G2 phase arrest of the glioma cell cycle. Another important finding of this study was that TRPC6 regulates G2 phase progression likely via control of CDC25C expression.

Several studies have shown that TRPC6 channels are involved in cell proliferation, including pulmonary artery smooth muscle cells (68); vascular endothelial cells (69,70); and different types of cancer cells, like prostate, breast, liver, and brain (24–27,71–73). In addition, TRPC1 channels play a role in proliferation of breast cancer cells (22) and mouse astrocytes (74), and TRPC3 channels are involved in proliferation of ovary and breast cancer cells (23,24).

Although it is well established that TRPC6 plays a role in cell proliferation in diverse cancer cells, it is not well understood whether TRPC6 channels regulate cell cycle progression to affect cell growth. A recent study demonstrated TRPC6 overexpression in tissue samples from GBM patients and suggested that TRPC6 was a key mediator of Notch-dependent glioblastoma growth and invasion (71). Here, we showed that TRPC6 affected glioma cell growth via regulation of G2 to M phase cell cycle progression.

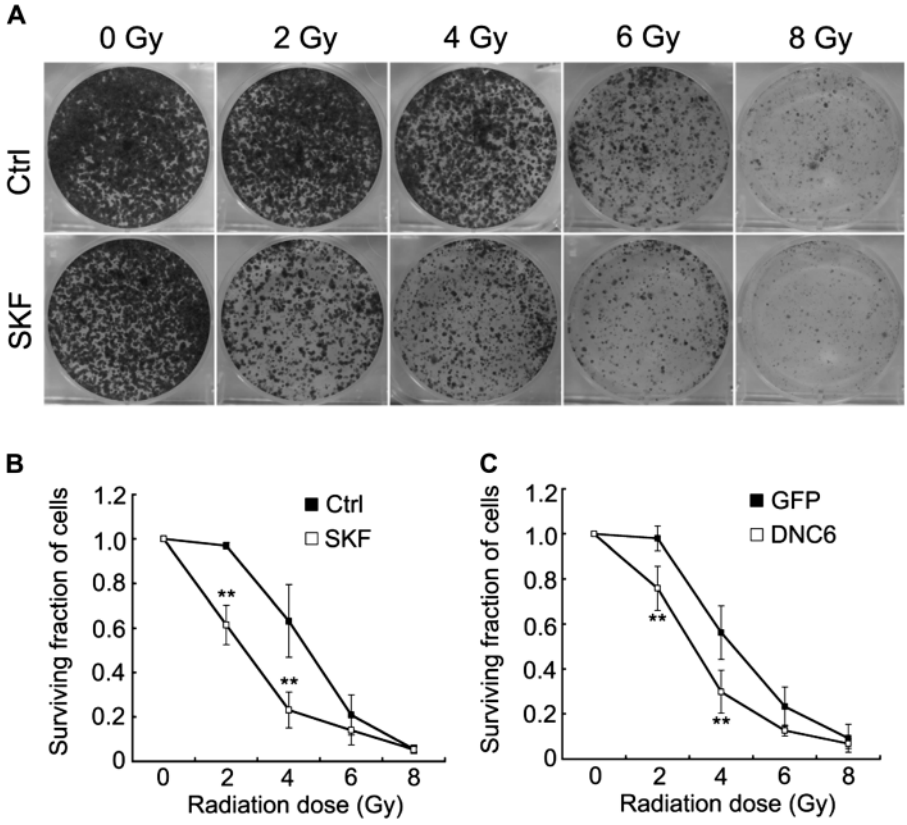

Figure 6. Effect of inhibition of transient receptor potential canonical 6 (TRPC6) activity on radiosensitization of glioma cells. **A**) Representative crystal violet staining of the colonies formed by U251 cells 11 days after irradiation with 0, 2, 4, 6, and 8 Gy. Cells were treated with vehicle (Ctrl) or 10 μM SKF96365 (SKF) 24 hours before irradiation. Ctrl = control. **B** and **C**) Surviving fraction of U251 cells after irradiation with 0, 2, 4, 6, and 8 Gy. Cells were treated with vehicle (Ctrl) or 10 μM SKF96365 (SKF) for 24 hours (**B**), or infected with adenovirus-based green fluorescent protein (GFP) or DNC6 at multiplicity of infection = 2, for 72 hours (**C**) before irradiation. Ctrl = control. Data were representative of five independent experiments, performed in duplicate. **Error bars** = 95% confidence interval. $^{**}P = .006$, SKF vs Ctrl at 2 Gy; $^{**}P = .005$, SKF vs Ctrl at 4 Gy; $^{**}P < .001$, GFP vs DNC6 at 2 Gy; $^{**}P = .002$, GFP vs DNC6 at 4 Gy. All *P* values were calculated using the two-sided Student *t* test.

Together, the results strongly suggest that TRPC6 plays a critical role in glioma development. Studies by Bomben and Sontheimer (25) showed that treatment with SKF96365 induced M phase arrest in glioma cells, whereas in our system, inhibition of TRPC6 by DNC6 or shTRPC6 induced G2, but not M, phase arrest. The difference might be explained by the nonspecific effects of SKF96365, which also blocks various other types of Ca^{2+} channels (63,75–79).

Previously, we have shown that TRPC6 channels are involved in the growth of human gastric carcinoma (80) and esophageal squamous cell carcinoma (81). Inhibition of TRPC6 channels in these human cancer cells suppressed cell proliferation and arrested cell cycle in the G2/M phase. These findings in different types of tumors indicate that TRPC6 is likely a key regulator of Ca^{2+}-mediated cell cycle progression. The current study on glioma cells further advanced these previous findings in several aspects. First, CDC25C is an essential regulator of G2/M transition (39), with a peak mRNA level at the G2 phase (82). Although CDC25C activation by phosphorylation has been extensively studied (39,83), whether Ca^{2+} signaling is involved in regulating its expression remains unknown. In this study, we showed that CDC25C transcription was regulated by TRPC6 channels but not by VGCCs. Illustration of signaling molecules downstream of TRPC6 will offer a better understanding of how Ca^{2+} signaling regulates G2 phase progression, a critical phase in the cell cycle for maintaining genomic stability (84). Second, it is well known that TRPC6 can be activated either by a receptor-operated pathway or by a store-operated pathway (19,28). We showed that in glioma cells, TRPC6 channels were activated by a store-operated pathway. Third, because cells are most radiosensitive in the G2/M phase of the cell cycle, enhanced radiosensitivity upon inhibition of TRPC6 channels in glioma cells supported the role of TRPC6 in G2/M phase progression. In addition, because radiotherapy is beneficial for the treatment of glioma, our results may provide a novel target for therapeutic intervention. Fourth, the intracranial glioma model, which is better than the subcutaneous model, produced additional convincing in vivo data and reinforced the importance of TRPC6 channels in glioma growth.

In normal cells, the G2 phase DNA damage checkpoint ensures genomic stability (84–86); however, cells with an impaired DNA damage checkpoint will develop genomic instability (87,88). It is possible that increased expression of TRPC6 in glioma cells accelerates G2 phase progression, and the cells override the DNA damage checkpoint as a result. Bypassing this checkpoint may facilitate the accumulation of mutations in the DNA and enhance glioma cell malignancy. However, we did not observe any gain-of-function effect when we infected glioma cells with WTC6. It is possible that the endogenous TRPC6 levels are high and channels are already saturated such that induced expression of more TRPC6 channels would not mediate more Ca^{2+} entry. Indeed, in Ca^{2+} imaging experiments, PDGF-induced $[Ca^{2+}]_i$ elevation in WTC6-infected cells was similar to that of control cells.

Our study has a few limitations. It did not address whether the homotetrameric or heterotetrameric form of TRPC6 affects glioma cell proliferation. It is possible that TRPC6 channels function as homotetramers; however, because TRPC3 is also expressed in the glioma cells, TRPC6 may also function as heterotetramers

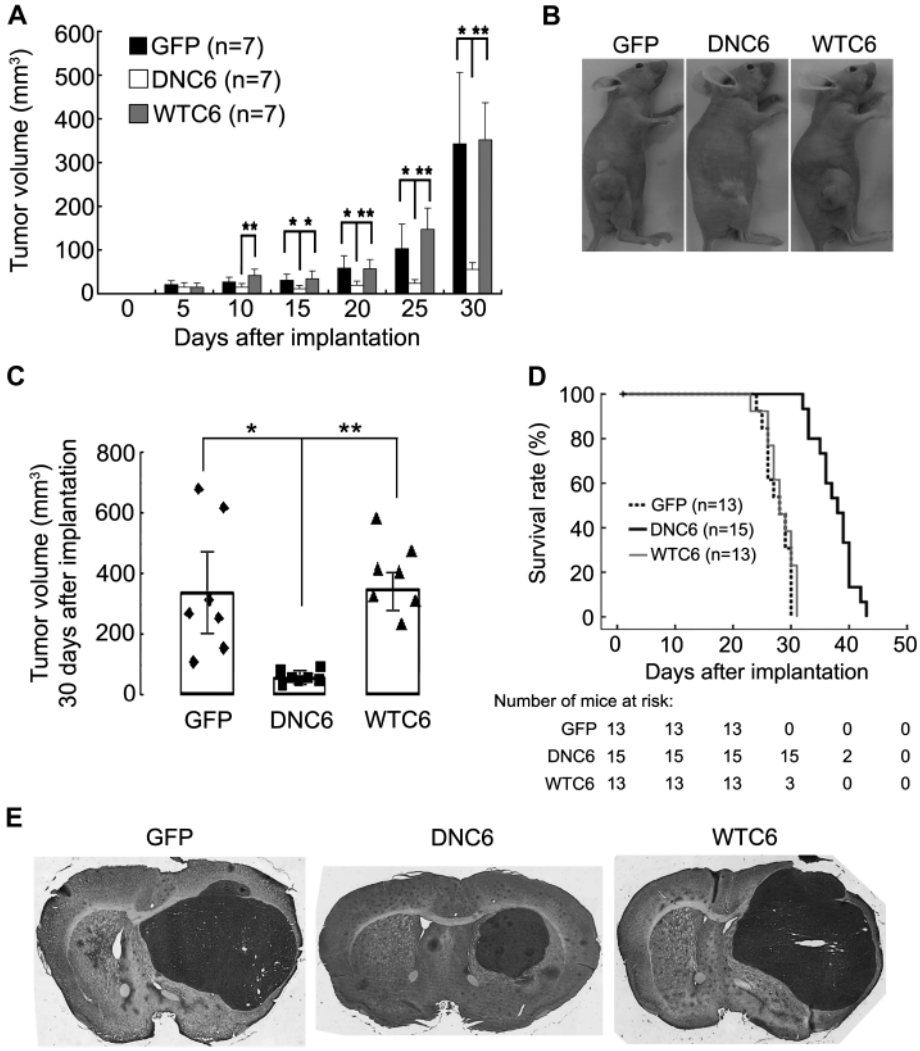

Figure 7. Effect of inhibition of transient receptor potential canonical 6 (TRPC6) activity on the development of xenografted human glioma. **A**) The tumor volumes in green fluorescent protein (GFP)-, DNC6-, and WTC6-infected groups (n = 7 per group) were determined every 5 days for 30 days after implantation of U87 cells. Means and upper 95% confidence intervals were shown. $*P < .05$, $**P < .01$, GFP or WTC6 vs DNC6. *P* values were calculated using the two-sided Student *t* test. **B**) Representative photographs of nude mice bearing xenografted tumors on day 30 of implantation. **C**) Scatter diagram of individual tumor volume of xenografted tumors on day 30 of implantation. Each symbol represents a single tumor. **Error bars** represent the interquartile range. $*P = .014$, GFP vs DNC6, $**P < .001$ WTC6 vs DNC6. *P* values were calculated using the two-sided Student *t* test. **D**) Survival curve was plotted by Kaplan–Meier analysis. Mice bearing glioma from DNC6-infected U87 cells survived longer than GFP- or WTC6-infected U87 cells. The number of mice (n) in each group is indicated. Each curve was compared using the two-sided log-rank test. $P < .001$, DNC6 vs GFP or WTC6. Number of mice at risk at each time point is also shown. **E**) Hematoxylin and eosin staining of representative coronal sections of the mouse brains 20 days after implantation. The tumors were derived from GFP-, DNC6-, and WTC6-infected U87 cells, respectively.

(50,89) to regulate cell cycle and glioma development. We would also like to point out that the signaling molecules downstream of TRPC6 that regulate CDC25C expression are not known. Identification of the signaling pathways downstream of TRPC6 that are involved in cell proliferation will provide a better understanding of how Ca^{2+} regulates G2/M phase transition in glioma cells. Additionally, we did not investigate whether inhibition of TRPC6 activity showed enhanced radiosensitivity in mice intracranially implanted with glioma.

In summary, the data presented in this study imply that TRPC6 channels may be a potential therapeutic target to treat human glioma. It is noteworthy that TRPC6 is also expressed in neurons and is important for neuronal functions (34–36). Therefore, a possible side effect of TRPC6 blockade on neurons must be considered. The adenovirus vector expressing DNC6 used in this study showed a very high affinity for glioma cells but a very low affinity for neurons (data not shown). Therefore, it is possible to reduce the potential side effects of TRPC6 inhibition on neurons using such adenovirus vectors. Additionally, because TRPC6 expression was barely detectable in normal glial cells, inhibition of TRPC6 in glioma cells likely has limited potential side effects on normal glial cells.

Supplementary Data

Supplementary data can be found at http://www.jnci.oxfordjournals.org/.

References

1. Sanai N, Alvarez-Buylla A, Berger MS. Neural stem cells and the origin of gliomas. *N Engl J Med.* 2005;353(8):811–822.
2. Behin A, Hoang-Xuan K, Carpentier AF, Delattre JY. Primary brain tumours in adults. *Lancet.* 2003;361(9354):323–331.
3. DeAngelis LM. Brain tumors. *N Engl J Med.* 2001;344(2):114–123.
4. Louis DN, Ohgaki H, Wiestler OD, et al. The 2007 WHO classification of tumours of the central nervous system. *Acta Neuropathol.* 2007;114(2):97–109.
5. Wen PY, Kesari S. Malignant gliomas in adults. *N Engl J Med.* 2008;359(5):492–507.
6. Legler JM, Gloeckler Ries LA, Smith MA, et al. Brain and other central nervous system cancers: recent trends in incidence and mortality. *J Natl Cancer Inst.* 1999;91(16):1382–1390.
7. Stark AM, Nabavi A, Mehdorn HM, Blomer U. Glioblastoma multiforme—report of 267 cases treated at a single institution. *Surg Neurol.* 2005;63(2):162–169. Discussion 169.
8. Berridge MJ, Bootman MD, Roderick HL. Calcium signalling: dynamics, homeostasis and remodelling. *Nat Rev Mol Cell Biol.* 2003;4(7):517–529.
9. Fiske JL, Fomin VP, Brown ML, Duncan RL, Sikes RA. Voltage-sensitive ion channels and cancer. *Cancer Metastasis Rev.* 2006;25(3):493–500.

10. Pardo LA, Contreras-Jurado C, Zientkowska M, Alves F, Stuhmer W. Role of voltage-gated potassium channels in cancer. *J Membr Biol.* 2005;205(3):115–124.
11. Kahl CR, Means AR. Regulation of cell cycle progression by calcium/calmodulin-dependent pathways. *Endocr Rev.* 2003;24(6):719–736.
12. Griner EM, Kazanietz MG. Protein kinase C and other diacylglycerol effectors in cancer. *Nat Rev Cancer.* 2007;7(4):281–294.
13. Roderick HL, Cook SJ. Ca2+ signalling checkpoints in cancer: remodelling Ca2+ for cancer cell proliferation and survival. *Nat Rev Cancer.* 2008;8(5):361–375.
14. Hofmann J. Protein kinase C isozymes as potential targets for anticancer therapy. *Curr Cancer Drug Targets.* 2004;4(2):125–146.
15. Rodriguez-Mora OG, LaHair MM, McCubrey JA, Franklin RA. Calcium/calmodulin-dependent kinase I and calcium/calmodulin-dependent kinase kinase participate in the control of cell cycle progression in MCF-7 human breast cancer cells. *Cancer Res.* 2005;65(12):5408–5416.
16. Lu F, Chen H, Zhou C, et al. T-type Ca2+ channel expression in human esophageal carcinomas: a functional role in proliferation. *Cell Calcium.* 2008;43(1):49–58.
17. Prevarskaya N, Zhang L, Barritt G. TRP channels in cancer. *Biochim Biophys Acta.* 2007;1772(8):937–946.
18. Wang XT, Nagaba Y, Cross HS, Wrba F, Zhang L, Guggino SE. The mRNA of L-type calcium channel elevated in colon cancer: protein distribution in normal and cancerous colon. *Am J Pathol.* 2000;157(5):1549–1562.
19. Montell C. The TRP superfamily of cation channels. *Sci STKE.* 2005;2005(272):re3.
20. Tai Y, Feng S, Du W, Wang Y. Functional roles of TRPC channels in the developing brain. *Pflugers Arch.* 2009;458(2):283–289.
21. Tiruppathi C, Minshall RD, Paria BC, Vogel SM, Malik AB. Role of Ca2+ signaling in the regulation of endothelial permeability. *Vascul Pharmacol.* 2002;39(4–5):173–185.
22. El Hiani Y, Ahidouch A, Lehen'kyi V, et al. Extracellular signal-regulated kinases 1 and 2 and TRPC1 channels are required for calcium-sensing receptor-stimulated MCF-7 breast cancer cell proliferation. *Cell Physiol Biochem.* 2009;23(4–6):335–346.
23. Yang SL, Cao Q, Zhou KC, Feng YJ, Wang YZ. Transient receptor potential channel C3 contributes to the progression of human ovarian cancer. *Oncogene.* 2009;28(10):1320–1328.
24. Aydar E, Yeo S, Djamgoz M, Palmer C. Abnormal expression, localization and interaction of canonical transient receptor potential ion channels in human breast cancer cell lines and tissues: a potential target for breast cancer diagnosis and therapy. *Cancer Cell Int.* 2009;9:23.
25. Bomben VC, Sontheimer HW. Inhibition of transient receptor potential canonical channels impairs cytokinesis in human malignant gliomas. *Cell Prolif.* 2008;41(1):98–121.
26. El Boustany C, Bidaux G, Enfissi A, Delcourt P, Prevarskaya N, Capiod T. Capacitative calcium entry and transient receptor potential canonical 6 expression control human hepatoma cell proliferation. *Hepatology.* 2008;47(6):2068–2077.
27. Thebault S, Flourakis M, Vanoverberghe K, et al. Differential role of transient receptor potential channels in Ca2+ entry and proliferation of prostate cancer epithelial cells. *Cancer Res.* 2006;66(4):2038–2047.
28. Ramsey IS, Delling M, Clapham DE. An introduction to TRP channels. *Annu Rev Physiol.* 2006;68:619–647.
29. Bolotina VM, Csutora P. CIF and other mysteries of the store-operated Ca2+-entry pathway. *Trends Biochem Sci.* 2005;30(7):378–387.
30. Abdullaev IF, Bisaillon JM, Potier M, Gonzalez JC, Motiani RK, Trebak M. Stim1 and Orai1 mediate CRAC currents and store-operated calcium entry important for endothelial cell proliferation. *Circ Res.* 2008;103(11):1289–1299.
31. Rozengurt E. Mitogenic signaling pathways induced by G protein-coupled receptors. *J Cell Physiol.* 2007;213(3):589–602.
32. Shih AH, Holland EC. Platelet-derived growth factor (PDGF) and glial tumorigenesis. *Cancer Lett.* 2006;232(2):139–147.
33. Turner N, Grose R. Fibroblast growth factor signalling: from development to cancer. *Nat Rev Cancer.* 2010;10(2):116–129.
34. Tai Y, Feng S, Ge R, et al. TRPC6 channels promote dendritic growth via the CaMKIV-CREB pathway. *J Cell Sci.* 2008;121(pt 14):2301–2307.
35. Zhou J, Du W, Zhou K, et al. Critical role of TRPC6 channels in the formation of excitatory synapses. *Nat Neurosci.* 2008;11(7):741–743.
36. Jia Y, Zhou J, Tai Y, Wang Y. TRPC channels promote cerebellar granule neuron survival. *Nat Neurosci.* 2007;10(5):559–567.
37. Pearson G, Robinson F, Beers Gibson T, et al. Mitogen-activated protein (MAP) kinase pathways: regulation and physiological functions. *Endocr Rev.* 2001;22(2):153–183.
38. Patel R, Holt M, Philipova R, et al. Calcium/calmodulin-dependent phosphorylation and activation of human Cdc25-C at the G2/M phase transition in HeLa cells. *J Biol Chem.* 1999;274(12):7958–7968.
39. Boutros R, Lobjois V, Ducommun B. CDC25 phosphatases in cancer cells: key players? Good targets? *Nat Rev Cancer.* 2007;7(7):495–507.
40. de Groot JF, Liu TJ, Fuller G, Yung WK. The excitatory amino acid transporter-2 induces apoptosis and decreases glioma growth in vitro and in vivo. *Cancer Res.* 2005;65(5):1934–1940.
41. Driessens G, Harsan L, Robaye B, et al. Micronuclei to detect in vivo chemotherapy damage in a p53 mutated solid tumour. *Br J Cancer.* 2003;89(4):727–729.
42. Furnari FB, Lin H, Huang HS, Cavenee WK. Growth suppression of glioma cells by PTEN requires a functional phosphatase catalytic domain. *Proc Natl Acad Sci U S A.* 1997;94(23):12479–12484.
43. Park CM, Park MJ, Kwak HJ, et al. Ionizing radiation enhances matrix metalloproteinase-2 secretion and invasion of glioma cells through Src/epidermal growth factor receptor-mediated p38/Akt and phosphatidylinositol 3-kinase/Akt signaling pathways. *Cancer Res.* 2006;66(17):8511–859.
44. Yin D, Zhou H, Kumagai T, et al. Proteasome inhibitor PS-341 causes cell growth arrest and apoptosis in human glioblastoma multiforme (GBM). *Oncogene.* 2005;24(3):344–354.
45. Demaurex N, Lew DP, Krause KH. Cyclopiazonic acid depletes intracellular Ca2+ stores and activates an influx pathway for divalent cations in HL-60 cells. *J Biol Chem.* 1992;267(4):2318–2324.
46. Wei Y, Yu L, Bowen J, Gorovsky MA, Allis CD. Phosphorylation of histone H3 is required for proper chromosome condensation and segregation. *Cell.* 1999;97(1):99–109.
47. Bartkova J, Horejsi Z, Koed K, et al. DNA damage response as a candidate anti-cancer barrier in early human tumorigenesis. *Nature.* 2005;434(7035):864–870.
48. Kleinschmidt-DeMasters BK, Orr EA, Savelieva E, Owens GC, Kruse CA. Paucity of retinoic acid receptor alpha (RAR alpha) nuclear immunostaining in gliomas and inability of retinoic acid to influence neural cell adhesion molecule (NCAM) expression. *J Neurooncol.* 1999;41(1):31–42.
49. Zhang Y, Zhang N, Dai B, et al. FoxM1B transcriptionally regulates vascular endothelial growth factor expression and promotes the angiogenesis and growth of glioma cells. *Cancer Res.* 2008;68(21):8733–8742.
50. Hofmann T, Schaefer M, Schultz G, Gudermann T. Subunit composition of mammalian transient receptor potential channels in living cells. *Proc Natl Acad Sci U S A.* 2002;99(11):7461–7466.
51. Rubinson DA, Dillon CP, Kwiatkowski AV, et al. A lentivirus-based system to functionally silence genes in primary mammalian cells, stem cells and transgenic mice by RNA interference. *Nat Genet.* 2003;33(3):401–406.
52. Fidler IJ. Rationale and methods for the use of nude mice to study the biology and therapy of human cancer metastasis. *Cancer Metastasis Rev.* 1986;5(1)29–49.
53. Clynes RA, Towers TL, Presta LG, Ravetch JV. Inhibitory Fc receptors modulate in vivo cytotoxicity against tumor targets. *Nat Med.* 2000;6(4):443–446.
54. Harding TC, Lalani AS, Roberts BN, et al. AAV serotype 8-mediated gene delivery of a soluble VEGF receptor to the CNS for the treatment of glioblastoma. *Mol Ther.* 2006;13(5):956–966.
55. Rustamzadeh E, Hall WA, Todhunter DA, et al. Intracranial therapy of glioblastoma with the fusion protein DTIL13 in immunodeficient mice. *Int J Cancer.* 2006;118(10):2594–2601.

56. Wilcox ME, Yang W, Senger D, et al. Reovirus as an oncolytic agent against experimental human malignant gliomas. *J Natl Cancer Inst.* 2001; 93(12):903–912.
57. Servidei T, Riccardi A, Sanguinetti M, Dominici C, Riccardi R. Increased sensitivity to the platelet-derived growth factor (PDGF) receptor inhibitor STI571 in chemoresistant glioma cells is associated with enhanced PDGF-BB-mediated signaling and STI571-induced Akt inactivation. *J Cell Physiol.* 2006;208(1):220–228.
58. Li HS, Xu XZ, Montell C. Activation of a TRPC3-dependent cation current through the neurotrophin BDNF. *Neuron.* 1999;24(1):261–273.
59. Li Y, Jia YC, Cui K, et al. Essential role of TRPC channels in the guidance of nerve growth cones by brain-derived neurotrophic factor. *Nature.* 2005;434(7035):894–898.
60. Saqr HE, Guan Z, Yates AJ, Stokes BT. Mechanisms through which PDGF alters intracellular calcium levels in U-1242 MG human glioma cells. *Neurochem Int.* 1999;35(6):411–422.
61. Lievremont JP, Bird GS, Putney JW Jr. Mechanism of inhibition of TRPC cation channels by 2-aminoethoxydiphenylborane. *Mol Pharmacol.* 2005;68(3):758–762.
62. Yu Y, Sweeney M, Zhang S, et al. PDGF stimulates pulmonary vascular smooth muscle cell proliferation by upregulating TRPC6 expression. *Am J Physiol Cell Physiol.* 2003;284(2):C316–C330.
63. Clapham DE. SnapShot: mammalian TRP channels. *Cell.* 2007;129(1):220.
64. Bertolesi GE, Shi C, Elbaum L, et al. The Ca(2+) channel antagonists mibefradil and pimozide inhibit cell growth via different cytotoxic mechanisms. *Mol Pharmacol.* 2002;62(2):210–219.
65. Grana X, Reddy EP. Cell cycle control in mammalian cells: role of cyclins, cyclin dependent kinases (CDKs), growth suppressor genes and cyclin-dependent kinase inhibitors (CKIs). *Oncogene.* 1995;11(2):211–219.
66. Geard CR, Jones JM, Schiff PB. Taxol and radiation. *J Natl Cancer Inst Monogr.* 1993;15:89–94.
67. Tishler RB, Schiff PB, Geard CR, Hall EJ. Taxol: a novel radiation sensitizer. *Int J Radiat Oncol Biol Phys.* 1992;22(3):613–617.
68. Yu Y, Fantozzi I, Remillard CV, et al. Enhanced expression of transient receptor potential channels in idiopathic pulmonary arterial hypertension. *Proc Natl Acad Sci U S A.* 2004;101(38):13861–13866.
69. Ge R, Tai Y, Sun Y, et al. Critical role of TRPC6 channels in VEGF-mediated angiogenesis. *Cancer Lett.* 2009;283(1):43–51.
70. Hamdollah Zadeh MA, Glass CA, Magnussen A, Hancox JC, Bates DO. VEGF-mediated elevated intracellular calcium and angiogenesis in human microvascular endothelial cells in vitro are inhibited by dominant negative TRPC6. *Microcirculation.* 2008;15(7):605–614.
71. Chigurupati S, Venkataraman R, Barrera D, et al. Receptor channel TRPC6 is a key mediator of Notch-driven glioblastoma growth and invasiveness. *Cancer Res.* 2010;70(1):418–427.
72. Guilbert A, Dhennin-Duthille I, Hiani YE, et al. Expression of TRPC6 channels in human epithelial breast cancer cells. *BMC Cancer.* 2008;8:125.
73. Yue D, Wang Y, Xiao JY, Wang P, Ren CS. Expression of TRPC6 in benign and malignant human prostate tissues. *Asian J Androl.* 2009;11(5): 541–547.
74. Golovina VA. Visualization of localized store-operated calcium entry in mouse astrocytes. Close proximity to the endoplasmic reticulum. *J Physiol.* 2005;564(pt 3):737–749.
75. Fiorio Pla A, Maric D, Brazer SC, et al. Canonical transient receptor potential 1 plays a role in basic fibroblast growth factor (bFGF)/FGF receptor-1-induced Ca2+ entry and embryonic rat neural stem cell proliferation. *J Neurosci.* 2005;25(10):2687–2701.
76. Kim SJ, Kim YS, Yuan JP, Petralia RS, Worley PF, Linden DJ. Activation of the TRPC1 cation channel by metabotropic glutamate receptor mGluR1. *Nature.* 2003;426(6964):285–291.
77. Malkia A, Madrid R, Meseguer V, et al. Bidirectional shifts of TRPM8 channel gating by temperature and chemical agents modulate the cold sensitivity of mammalian thermoreceptors. *J Physiol.* 2007;581(pt 1): 155–174.
78. Merritt JE, Armstrong WP, Benham CD, et al. SK&F 96365, a novel inhibitor of receptor-mediated calcium entry. *Biochem J.* 1990;271(2): 515–522.
79. Vazquez G, Wedel BJ, Aziz O, Trebak M, Putney JW Jr. The mammalian TRPC cation channels. *Biochim Biophys Acta.* 2004;1742(1–3): 21–36.
80. Cai R, Ding X, Zhou K, et al. Blockade of TRPC6 channels induced G2/M phase arrest and suppressed growth in human gastric cancer cells. *Int J Cancer.* 2009;125(10):2281–2287.
81. Shi Y, Ding X, He ZH, Zhou KC, Wang Q, Wang YZ. Critical role of TRPC6 channels in G2 phase transition and the development of human oesophageal cancer. *Gut.* 2009;58(11):1443–1450.
82. Sadhu K, Reed SI, Richardson H, Russell P. Human homolog of fission yeast cdc25 mitotic inducer is predominantly expressed in G2. *Proc Natl Acad Sci U S A.* 1990;87(13):5139–5143.
83. Wang R, He G, Nelman-Gonzalez M, et al. Regulation of Cdc25C by ERK-MAP kinases during the G2/M transition. *Cell.* 2007;128(6): 1119–1132.
84. Sancar A, Lindsey-Boltz LA, Unsal-Kacmaz K, Linn S. Molecular mechanisms of mammalian DNA repair and the DNA damage checkpoints. *Annu Rev Biochem.* 2004;73:39–85.
85. Bartek J, Lukas J. DNA damage checkpoints: from initiation to recovery or adaptation. *Curr Opin Cell Biol.* 2007;19(2):238–245.
86. Harper JW, Elledge SJ. The DNA damage response: ten years after. *Mol Cell.* 2007;28(5):739–745.
87. Kastan MB, Bartek J. Cell-cycle checkpoints and cancer. *Nature.* 2004;432(7015):316–323.
88. Lobrich M, Jeggo PA. The impact of a negligent G2/M checkpoint on genomic instability and cancer induction. *Nat Rev Cancer.* 2007;7(11): 861–869.
89. Goel M, Sinkins WG, Schilling WP. Selective association of TRPC channel subunits in rat brain synaptosomes. *J Biol Chem.* 2002;277(50): 48303–48310.

Funding

This work was supported by grants from the 973 Program (2006CB806600) (YZW) and project 30711120566 (Y.W.) from the National Natural Science Foundation of China.

Notes

X. Ding, Z. He, and K. Zhou contributed equally to this work.

X. Ding, Z. He, and K. Zhou designed and conducted the experiments and wrote the manuscript. J. Cheng performed in situ hybridization. H. Yao and D. Lu helped with immunoblot and PCR experiments. R. Cai, B. Dong, Y. Xu, and Y. Jin helped with radiosensitization experiments. Y. Wang supervised the project and wrote the manuscript.

We thank T. Gudermann (Walther-Straub-Institut of Pharmacology and Toxicology, Ludwig-Maximilians-Universitaet Muenchen, Germany) for wild-type TRPC6, M. Sendtner (Institute for Clinical Neurobiology, Wuerzburg, Germany) for lentiviral vectors, and H. He (Ruijin Hospital, Jiaotong University School of Medicine, Shanghai, China) for human clinical samples.

Affiliations of authors: Laboratory of Neural Signal Transduction, Institute of Neuroscience, Shanghai Institute for Biological Sciences, State Key Laboratory of Neuroscience (XD, ZH, KZ, JC, HY, DL, YW) and Graduate School (XD, ZH, KZ, JC, HY, DL), Chinese Academy of Sciences, Shanghai, China; Ruijin Hospital, Department of Radiochemotherapy, Jiaotong University School of Medicine, Shanghai, China (RC, YJ); Department of Neurosurgery, First Affiliated Hospital of Dalian Medical University, Dalian, China (BD, YX).